Impaired intracellular Ca^{2+} signaling contributes to age-related cerebral small vessel disease in *Col4a1* mutant mice

Evan Yamasaki[1], Pratish Thakore[1], Sher Ali[1], Alfredo Sanchez Solano[1], Xiaowei Wang[2], Xiao Gao[3,4], Cassandre Labelle-Dumais[2], Myriam M. Chaumeil[3,4], Douglas B. Gould[2,5], and Scott Earley[1*]

[1]Department of Pharmacology, Center for Molecular and Cellular Signaling in the Cardiovascular System, University of Nevada, Reno School of Medicine, Reno, NV 89557-0318, USA

[2]Department of Ophthalmology, UCSF School of Medicine, San Francisco, CA 94158, USA

[3]Department of Physical Therapy and Rehabilitation Science, UCSF School of Medicine, San Francisco, CA 94143, USA

[4]Department of Radiology and Biomedical Imaging, UCSF School of Medicine, San Francisco, CA 94143, USA

[5]Department of Anatomy, Institute for Human Genetics, Cardiovascular Research Institute, Bakar Aging Research Institute, UCSF School of Medicine, San Francisco, CA 94158, USA

Keywords: *COL4A1*, collagen, cerebral small vessel diseases, basement membrane, myogenic tone, TRPM4, IP_3R, Calcium, Ca^{2+}, ER Stress, SR Stress, ion channels.

[*]Corresponding author

Address Correspondence To: Scott Earley, Ph.D.
University of Nevada, Reno School of Medicine
Manville Health Sciences Building, Room 8
MS-0318
Reno, NV 89557-0318, USA
Phone: (775) 784-4117
Fax: (775) 784-1620
Email: searley@med.unr.edu

Abstract

Humans and mice with mutations in *COL4A1* and *COL4A2* manifest hallmarks of cerebral small vessel disease (cSVD), but the pathogenic mechanisms are largely unknown. Mice with a missense mutation in *Col4a1* at amino acid 1344 (*Col4a1*$^{+/G1344D}$) exhibited age-dependent intracerebral hemorrhage (ICH) and brain lesions. Here we report that this pathology was associated with the loss of myogenic vasoconstriction, an intrinsic vascular response essential for the autoregulation of cerebral blood flow. Electrophysiological analyses showed that the loss of myogenic constriction resulted from blunted pressure-induced smooth muscle cell (SMC) membrane depolarization. Further, we found that dysregulation of membrane potential was associated with impaired Ca^{2+}-dependent activation of large-conductance Ca^{2+}-activated K^+ (BK) and transient receptor potential melastatin 4 (TRPM4) cation channels linked to disruptions in sarcoplasmic reticulum (SR) Ca^{2+} signaling. Treating *Col4a1*$^{+/G1344D}$ mice with 4-phenylbutyrate, a compound that promotes the trafficking of misfolded proteins and alleviates SR stress, restored SR Ca^{2+} signaling, BK and TRPM4 channel activity, prevented loss of myogenic tone, and reduced ICH. We conclude that alterations in SR Ca^{2+} handling that impair membrane potential regulating ion channel activity result in dysregulation of SMC membrane potential and loss of myogenic tone contributing to age-related cSVD in *Col4a1*$^{+/G1344D}$ mice.

56 **Graphical Abstract**

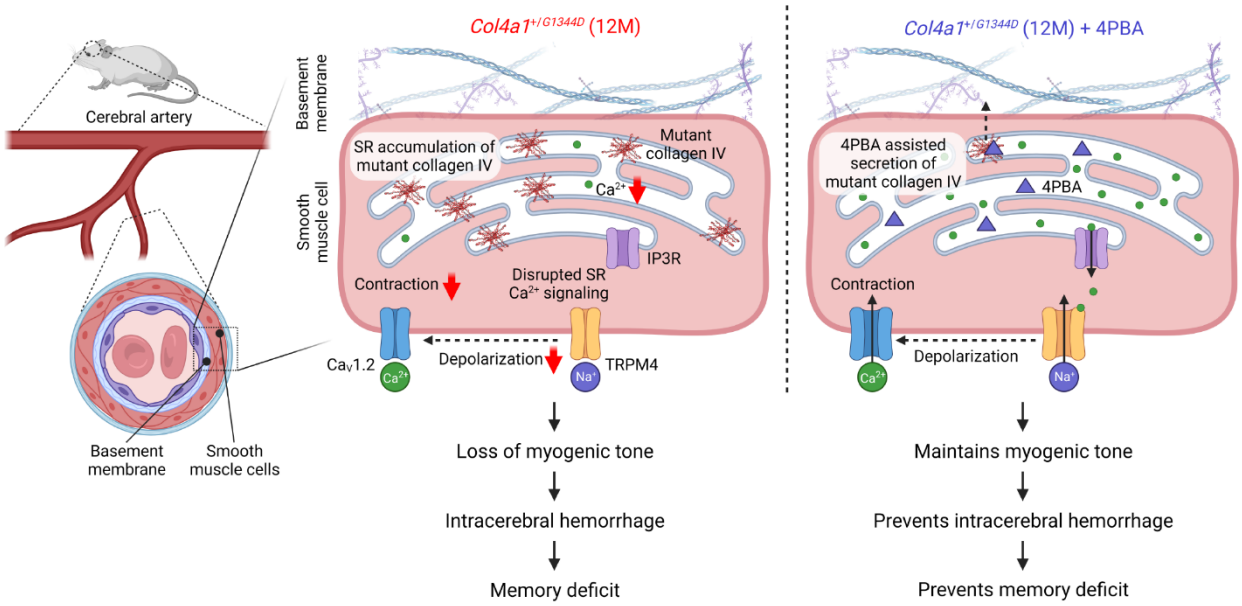

57

58

59

60 **Introduction**

61 Cerebral small vessel diseases (cSVDs) are a group of related pathologies that
62 damage arteries, arterioles, venules, and capillaries in the brain. cSVDs constitute a
63 significant cause of stroke and, after Alzheimer's disease, are the second leading cause
64 of adult cognitive impairment and dementia [1,2]. The underlying pathogenic mechanisms
65 remain largely unknown, and no specific treatment options exist. Sporadic and familial
66 forms of cSVD share clinical and radiological features, including white matter
67 hyperintensities, dilated perivascular spaces, lacunar infarcts, microbleeds, and
68 intracerebral hemorrhages (ICHs) [3-6]. Individuals with Gould syndrome, a rare
69 multisystem disorder caused by autosomal dominant mutations in collagen IV alpha 1
70 (*COL4A1*) and alpha 2 (*COL4A2*), manifest these hallmarks [7-9]. The majority of
71 pathogenic *COL4A1* and *COL4A2* mutations substitute critical glycine (G) residues
72 within triple helical domains [10]. These mutations have several deleterious effects,
73 including impaired secretion of mature COL4A1 and COL4A2 heterotrimers
74 [$\alpha1\alpha1\alpha2$(IV)] that form basement membranes and intracellular retention of mutant
75 collagen that can lead to endoplasmic reticulum (ER) stress [11-13]. However, it is unclear
76 how these defects influence the pathology of cSVD. *Col4a1* and *Col4a2* mutations
77 demonstrate position-dependent effects contributing to phenotypic heterogeneity [13]. For
78 the current study, we investigated the pathogenesis of *Col4a1*-associated cSVD using
79 mice with a missense mutation that changes the G residue at amino acid position 1344
80 to aspartate (D). These animals, designated *Col4a1*$^{+/G1344D}$, model the most common
81 type of mutation in humans and develop severe cSVD pathology compared to other

82 mutant mice carrying glycine missense mutations in a murine allelic series of *Col4a1*
83 and *Col4a2* mutations [10,13].

84 Distinctive attributes of the cerebral vasculature serve the unique requirements of
85 the brain. For example, cerebral arteries and arterioles exhibit graded constriction in
86 response to changes in intravascular pressure. This vital autoregulatory process, known
87 as the vascular myogenic response, protects downstream capillary beds from potentially
88 harmful increases in perfusion pressure when cardiac output is transiently elevated
89 during exercise or other stimuli [14]. The myogenic response is intrinsic to vascular
90 smooth muscle cells (SMCs) and requires the coordinated activity of several ion
91 channels. Increases in intraluminal pressure activate transient receptor potential
92 melastatin 4 (TRPM4) channels, allowing an influx of Na^+ ions that depolarizes the
93 plasma membrane to increase voltage-dependent Ca^{2+} inflow through Cav1.2 Ca^{2+}
94 channels and engage the contractile apparatus [15,16]. Knockdown studies of TRPM4
95 show that *in vivo* suppression of TRPM4 decreases cerebral artery myogenic
96 constriction and impairs cerebral blood flow autoregulation [17]. Pressure-induced
97 membrane depolarization is balanced by hyperpolarizing currents conducted by several
98 K^+-permeable ion channels, including large-conductance Ca^{2+}-activated K^+ (BK)
99 channels, voltage-dependent K^+ (K_V) channels, and others [18-20]. The interplay of
100 depolarizing and hyperpolarizing currents controls the resting membrane potential of
101 SMCs and maintains cerebral arteries in a state of partial contraction. BK and TRPM4
102 channels require high levels of intracellular Ca^{2+} for activation and, under native
103 conditions, are stimulated by Ca^{2+} released from the sarcoplasmic reticulum (SR)
104 through ryanodine receptors (RyRs) and inositol trisphosphate receptors (IP_3Rs),

105 respectively [18,21]. Impairment of the myogenic response has been implicated in many
106 types of cerebrovascular disease, including familial cSVDs associated with cerebral
107 autosomal dominant arteriopathy with subcortical infarcts and leukoencephalopathy
108 (CADASIL) caused by mutations in *NOTCH3* [22]. However, the impact of the
109 *Col4a1*^{G1344D} mutation on the myogenic response is not known.

110 Here, we report that *Col4a1*$^{+/G1344D}$ mice exhibit age-dependent loss of myogenic
111 tone that is associated with spontaneous intracerebral hemorrhage (ICH) and brain
112 lesions detected by susceptibility-weighted magnetic resonance imaging (SWI). The
113 deficit in myogenic tone resulted from diminished stretch-induced activation of TRPM4
114 channels and subsequent impairment of SMC membrane depolarization. We also
115 found that subcellular and global Ca^{2+} signals generated by releasing Ca^{2+} from the SR
116 through RyRs and IP_3Rs were disrupted in SMCs from aged *Col4a1*$^{+/G1344D}$ mice.
117 Treating *Col4a1*$^{+/G1344D}$ mice with 4-phenylbutyrate (4PBA), a small molecule with
118 chaperone properties that improves the secretion of misfolded proteins from the ER/SR
119 [10,13,23-26], prevented SR Ca^{2+} signaling defects, preserved TRPM4 channel activity,
120 attenuated the loss of myogenic tone, and largely protected mice from ICH. These data
121 provide evidence that accumulation of misfolded α1α1α2(IV) collagen in the SR of
122 SMCs from *Col4a1*$^{+/G1344D}$ mice causes disruptions in intracellular Ca^{2+} signaling,
123 stretch-induced activation of TRPM4 channels, pressure-induced SMC membrane
124 potential depolarization, and myogenic constriction. Our data also suggests these
125 defects contribute to spontaneous age-related ICH in *Col4a1*$^{+/G1344D}$ mice. Thus, the
126 findings of this study reveal a novel age-dependent facet of cSVD pathogenesis.

127 **Results**

128 ***Col4a1$^{+/G1344D}$* mice exhibit age-dependent pathology.**

129 All studies utilized *Col4a1$^{+/G1344D}$* mice and *Col4a1$^{+/+}$* littermates as controls.
130 *Col4a1$^{+/G1344D}$* mice carry missense mutation at amino acid 1344 near the C-terminus of
131 the triple helical domain (Figure 1A). Age is the most critical risk factor for cSVD and
132 vascular dementia [27,28]. To investigate age-related aspects of cSVD pathology, mice
133 were studied at 3 and at least 12 months (M) of age, representing the young adult and
134 middle age stages of life, respectively. Male and female mice were used throughout the
135 study, and no sex-specific differences were detected.

136 Spontaneous ICH is a highly penetrant and consequential manifestation of
137 *Col4a1* mutations that increases in severity with age [10,29,30]. ICH severity was measured
138 in brain sections from *Col4a1$^{+/+}$* and *Col4a1$^{+/G1344D}$* mice stained with Prussian blue.
139 ICH was not detected in 3 M-old *Col4a1$^{+/+}$* mice. Low-level, punctate Prussian blue
140 staining was present in brain sections from 3 M-old *Col4a1$^{+/G1344D}$* mice (Figure 1B and
141 C). 12 M-old *Col4a1$^{+/+}$* mice did not exhibit ICH, but brain sections from 12 M-old
142 *Col4a1$^{+/G1344D}$* mice displayed large areas of Prussian blue staining mainly localized to
143 the subcortical regions (Figure 1D and E). The total area of Prussian blue staining in 12
144 M-old *Col4a1$^{+/G1344D}$* mice was nearly 20-fold greater than in 3 M-old mutants (1.9% vs.
145 0.1% of brain area, respectively), indicating that the severity of spontaneous ICH
146 increases dramatically with age.

147 Neuroimaging is frequently used to diagnose cSVD in human patients [31]. In this
148 study, 12 M-old *Col4a1$^{+/+}$* and *Col4a1$^{+/G1344D}$* mice were evaluated using SWI. 12 M-old

149 *Col4a1*$^{+/+}$ mice did not exhibit SWI-detectable brain lesions, but brains from age-
150 matched *Col4a1*$^{+/G1344D}$ mice had multiple lesions, mainly localized to the thalamus
151 (Figure 1F-I). The number, total volume, and localization of brain lesions detected with
152 SWI are consistent with ICH detected with Prussian blue staining.

153

154 **Diminished pressure-induced constriction of cerebral arteries from 12 M-old**
155 ***Col4a1*$^{+/G1344D}$ mice is due to impaired SMC membrane depolarization.**

156 To better understand the underlying causes of ICH in *Col4a1*$^{+/G1344D}$ mice, we
157 used *ex vivo* pressure myography to study the myogenic response of cerebral arteries
158 [32]. Vasoconstriction in response to stepwise increases in intraluminal pressure (from 5
159 to 120 mmHg) was evaluated by measuring the active steady-state luminal diameter of
160 cannulated cerebral arteries bathed in standard physiological saline solution at each
161 pressure. This procedure was then repeated using a Ca^{2+}-free bathing solution to
162 determine the passive response to pressure, and myogenic tone was calculated as the
163 difference in active versus passive diameter normalized to the passive diameter. The
164 myogenic tone of cerebral arteries isolated from 3 M-old *Col4a1*$^{+/+}$ and *Col4a1*$^{+/G1344D}$
165 mice did not differ (Figure 2A and B). However, cerebral arteries from 12 M-old
166 *Col4a1*$^{+/G1344D}$ mice barely constricted in response to pressure and had significantly
167 lower levels of myogenic tone than those from age-matched *Col4a1*$^{+/+}$ mice (Figure 2C
168 and D).

169 Increases in intraluminal pressure cause SMCs in the vascular wall to depolarize
170 [33], triggering voltage-dependent Ca^{2+} influx and muscular contraction [33,34]. To

171 determine if the loss of myogenic tone in 12 M-old *Col4a1*$^{+/G1344D}$ mice was associated
172 with impaired pressure-induced depolarization, we recorded the membrane potentials of
173 SMCs in intact cerebral arteries using intracellular microelectrodes. At low intraluminal
174 pressure (20 mmHg), the membrane potential of SMCs in cerebral arteries from 3 M-old
175 *Col4a1*$^{+/+}$ and *Col4a1*$^{+/G1344D}$ mice did not differ (Figure 2E and F). Increasing
176 intraluminal pressure to physiological levels (80 mmHg) depolarized the SMC
177 membrane potential in arteries from both groups to the same extent (Figure 2E and F).
178 When vessels from 12 M-old animals were investigated, SMC membrane potential did
179 not differ between *Col4a1*$^{+/+}$ and *Col4a1*$^{+/G1344D}$ when arteries were pressurized to 20
180 mmHg (Figure 2G and H), but when intraluminal pressure was increased to 80 mmHg,
181 the depolarization of SMCs in cerebral arteries from *Col4a1*$^{+/G1344D}$ mice was
182 significantly blunted compared with controls (Figure 2G and H). These data suggest that
183 cerebral arteries from 12 M-old *Col4a1*$^{+/G1344D}$ mice lose myogenic tone because
184 pressure-induced SMC membrane depolarization is impaired.

185

186 **Age-dependent declines in BK and TRPM4 channel activity in SMCs from**
187 ***Col4a1*$^{+/G1344D}$ mice.**

188 To determine if changes in ion channel activity account for impaired pressure-
189 induced SMC depolarization, we used patch-clamp electrophysiology to compare
190 hyperpolarizing K_V and BK currents and depolarizing TRPM4 currents in native SMCs
191 from control and *Col4a1*$^{+/G1344D}$ mice.

192 Elevated SMC K_V channel current density is responsible for diminished myogenic
193 tone in cerebral arteries from CADASIL cSVD mice [22]. We measured K_V currents in
194 freshly isolated SMCs to determine if a similar mechanism accounts for the loss of
195 myogenic tone in cerebral arteries from 12 M-old *Col4a1*$^{+/G1344D}$ mice. K_V currents were
196 recorded using the amphotericin B perforated patch-clamp configuration to maintain the
197 integrity of intracellular signaling cascades. Whole-cell currents were evoked by
198 applying voltage steps from -60 to +60 mV from a holding potential of -80 mV in the
199 presence of selective BK channel blocker paxilline (1 μM). The voltage step protocol
200 was repeated in the presence of K_V channel blocker 4-aminopyridine (5 mM), and K_V
201 current amplitude was determined at each potential by subtraction. We found that K_V
202 current amplitudes did not differ between SMCs from 12 M-old *Col4a1*$^{+/+}$ and
203 *Col4a1*$^{+/G1344D}$ mice at all applied command potentials (Supplemental Figure 1A and B).

204 The activity of BK channels in cerebral artery SMCs under native conditions is
205 driven by the transient release of Ca^{2+} ions through RyRs on the SR into restricted
206 subcellular microdomains proximal to the plasma membrane [35]. These signaling events,
207 known as Ca^{2+} sparks, activate clusters of BK channels on the plasma membrane to
208 generate large-amplitude spontaneous transient outward currents (STOCs) [18,19]. We
209 utilized the amphotericin B perforated patch-clamp configuration to measure STOCs in
210 cerebral artery SMCs from 3 M-old *Col4a1*$^{+/+}$ and *Col4a1*$^{+/G1344D}$ mice over a range of
211 command potentials (-60 to 0 mV) and saw no significant difference in STOC frequency
212 or amplitude (Figure 3A-C). However, the frequency and amplitude of STOCs were
213 significantly lower in cerebral artery SMCs from 12 M-old *Col4a1*$^{+/G1344D}$ mice compared
214 with age-matched controls (Figure 3D-F). To determine if decreases in STOCs result

215 from changes in gene expression, we utilized ddPCR to measure transcript levels of
216 *Kcnma1* (BK subunit α), *Kcnmb1 (*BK subunit β1), and *Ryr2* (ryanodine receptor 2). No
217 differences in mRNA expression levels were detected (Supplemental Figure 2).

218 Reduced BK channel activity depolarizes the SMC membrane potential and
219 increases contractility [36]. Thus, diminished BK channel activity in SMCs from 12 M-old
220 *Col4a1*$^{+/G1344D}$ mice cannot account for impaired pressure-induced membrane
221 depolarization.

222 TRPM4 is a Ca^{2+}-activated, nonselective monovalent cation channel required for
223 pressure-induced SMC depolarization and the development of myogenic tone in
224 cerebral arteries [15,16,37,38]. At the membrane potentials of SMCs in the vascular wall
225 under physiological conditions (-60 to -30 mV), TRPM4 channels conduct inward Na^+
226 currents that depolarize the plasma membrane in response to increases in intraluminal
227 pressure [15,39]. Patch-clamp electrophysiology was used to determine if TRPM4 activity
228 is diminished in *Col4a1*$^{+/G1344D}$ mice. We assessed channel function and availability in
229 freshly isolated cerebral artery SMCs using the conventional whole-cell patch-clamp
230 configuration with a high [Ca^{2+}] intracellular solution to directly activate TRPM4.
231 Currents were recorded as voltage ramps (-100 to +100 mV) were applied. Voltage
232 ramps were repeated in the presence of TRPM4 blocker 9-phenanthrol (30 μM) [15], and
233 TRPM4 currents were isolated by subtraction. Prior studies using ion substitution
234 protocols have shown that Ca^{2+}-activated, 9-phenanthrol currents recorded using these
235 methods are carried by Na^+ ions, providing substantial evidence that these are *bona*
236 *fide* TRPM4 currents [16,37,40]. We found that the amplitudes of whole-cell TRPM4 currents
237 recorded from cerebral artery SMCs did not differ between *Col4a1*$^{+/+}$ and *Col4a1*$^{+/G1344D}$

238 mice at 3 and 12 M of age (Figure 3G-J). These data indicate that the collagen mutation
239 studied here has no direct effects on TRPM4 channel function or the trafficking of
240 channel protein to the plasma membrane.

241 TRPM4 channels in SMCs are activated by a signal transduction cascade
242 initiated by angiotensin II type 1 receptors (AT_1Rs) [41-44]. Activation of Gq protein-
243 coupled AT_1Rs stimulates phospholipase C (PLC), leading to the cleavage of
244 phosphatidylinositol 4,5-bisphosphate (PIP_2) into diacylglycerol and inositol triphosphate
245 (IP_3). IP_3 stimulates Ca^{2+} release from the SR through IP_3Rs to transiently activate
246 TRPM4 channels [21,38,41]. AT_1Rs are directly activated by the stretch of the plasma
247 membrane (independent of their ligand) and are a critical mechanosensor in SMCs [41-44].
248 To measure the activity of TRPM4 channels in response to mechanical force, we patch-
249 clamped SMCs in the amphotericin B perforated patch configuration and applied
250 negative pressure (-20 mmHg) through the patch pipet to stretch the plasma membrane.
251 Stretch-induced transient inward cation currents (TICCs) evoked in this manner are
252 blocked by 9-phenanthrol and abolished by the knockdown of TRPM4 expression [15,21].
253 Stretch-activated TICC activity in SMCs from 3 M-old *Col4a1*$^{+/+}$ and *Col4a1*$^{+/G1344D}$
254 (Figure 3K and L) did not differ. In contrast, stretch-induced TICC activity in SMCs from
255 12 M-old *Col4a1*$^{+/G1344D}$ mice was significantly lower than that of age-matched *Col4a1*$^{+/+}$
256 mice (Figure 3M and N). To determine if altered gene expression underlies the
257 reduction in TICC activity, we utilized ddPCR to measure transcript levels of *Trpm4*
258 (TRPM4), *Itpr1* (IP_3 receptor 1), and *Itpr2* (IP_3 receptor 2) in cerebral arteries from 12 M-
259 old *Col4a1*$^{+/+}$ and *Col4a1*$^{+/G1344D}$ mice. No differences in mRNA copy numbers were
260 observed (Supplemental Figure 2). These data suggest that blunted pressure-induced

261 SMC depolarization and impaired myogenic tone result from diminished stretch-induced
262 activation of TRPM4 channels.

263

264 **Defective intracellular Ca^{2+} signaling in cerebral artery SMCs from 12 M-old**
265 ***Col4a1*$^{+/G1344D}$ mice.**

266 Ca^{2+} released from the SR drives BK and TRPM4 channel activity in cerebral
267 artery SMCs [18,21]. Therefore, we investigated the possibility that these vital Ca^{2+}
268 signaling pathways are disrupted in SMCs from 12 M-old *Col4a1*$^{+/G1344D}$ mice. Freshly
269 isolated SMCs were loaded with the Ca^{2+}-sensitive fluorophore Fluo-4 AM and imaged
270 using high-speed, high-resolution spinning disk confocal microscopy. Spontaneous Ca^{2+}
271 sparks were present in SMCs isolated from 3 M-old *Col4a1*$^{+/+}$ and *Col4a1*$^{+/G1344D}$ mice.
272 The frequency, amplitude, duration, rise time, and decay rate did not differ between
273 groups (Figure 4A-C). Spontaneous Ca^{2+} sparks were also present in SMCs isolated
274 from both groups of 12 M-old mice. No significant differences in Ca^{2+} spark amplitude,
275 duration, rise time, and decay rate were observed, but notably, Ca^{2+} spark frequency
276 was significantly lower in SMCs from 12 M-old *Col4a1*$^{+/G1344D}$ mice (Figure 4D-F). Thus,
277 diminished Ca^{2+} spark frequency likely accounts for decreased STOC frequency in
278 SMCs from 12 M-old *Col4a1* mutant mice.

279 Fluo-4 AM-loaded SMCs were challenged with the RyR agonist caffeine (10 mM)
280 to investigate how RyR function was affected by the *Col4a1*^{G1344D} mutation [45]. Ca^{2+}
281 signals arising from intracellular release were isolated from Ca^{2+} influx events by acutely
282 removing Ca^{2+} from the extracellular solution immediately before recording. Caffeine-

283 evoked global cytosolic [Ca^{2+}] increases did not differ between SMCs from 3 M-old
284 *Col4a1*$^{+/+}$ and *Col4a1*$^{+/G1344D}$ mice (Figure 4G and H). In contrast, caffeine-induced
285 global Ca^{2+} signals were smaller in amplitude in SMCs from 12 M-old *Col4a1*$^{+/G1344D}$
286 mice than in controls (Figure 4I and J). These data indicate that the release of SR Ca^{2+}
287 from RyRs is impaired in the SMCs of *Col4a1*$^{+/G1344D}$ mice in an age-dependent manner.

288 Fluo-4 AM loaded-SMCs were also treated with the G_q protein-coupled
289 thromboxane A2 receptor agonist U46619 (100 nM) to investigate IP_3R-mediated Ca^{2+}
290 signaling. U46619-induced Ca^{2+} signals did not differ between cerebral artery SMCs
291 from 3 M-old *Col4a1*$^{+/+}$ and *Col4a1*$^{+/G1344D}$ mice (Figure 4K and L). In contrast, Ca^{2+}
292 signals induced by U46619 were smaller in amplitude in SMCs from 12 M-old
293 *Col4a1*$^{+/G1344D}$ mice compared to controls (Figure 4M and N). These data suggest that
294 the release of SR Ca^{2+} from IP_3Rs is also impaired in the SMCs of *Col4a1*$^{+/G1344D}$ mice
295 in an age-dependent manner.

296 RyRs and IP_3Rs share a common SR Ca^{2+} pool [46]. Impairment of Ca^{2+} release
297 through both receptors suggests that the SR [Ca^{2+}] of SMCs from 12 M-old
298 *Col4a1*$^{+/G1344D}$ mice is lower than that of corresponding controls. Further, diminished SR
299 Ca^{2+} levels likely account for decreased Ca^{2+} spark frequency and diminished STOC
300 and TICC activity.

301

302 **4PBA prevents age-related cerebral artery defects in *Col4a1*$^{+/G1344D}$ mice.**

303 *Col4a1* mutations impair collagen α1α1α2(IV) secretion *in vitro* and *in vivo* and
304 can be alleviated by treatment with 4PBA [10,13,26]. The chemical chaperone 4PBA

305 facilitates the trafficking of misfolded mutant proteins and reduces ER/SR stress [47]. To
306 investigate a potential link between impaired collagen secretion and the cerebral
307 vascular pathology of *Col4a1*$^{+/G1344D}$ mice, 4PBA (50 mM) was added to the drinking
308 water of mutant and control animals from birth (postnatal day 0).

309 We found that 4PBA treatment prevented the diminishment of caffeine-evoked
310 (Figure 5A and B) and U46619-induced (Figure 5C and D) Ca^{2+} signals in cerebral
311 artery SMCs from 12 M-old *Col4a1*$^{+/G1344D}$ mice. Ca^{2+} spark frequency was also
312 normalized to control levels in 4PBA-treated *Col4a1*$^{+/G1344D}$ mice (Supplemental Figure
313 3A-C). We also found that 4PBA treatment averted the loss of STOC (Supplemental
314 Figure 3D-E) and TICC (Figure 5E and F) activity. These data demonstrate that age-
315 related defects in intracellular Ca^{2+} signaling that control ion channel activity and
316 membrane potential were prevented by treating *Col4a1*$^{+/G1344D}$ mice with 4PBA. 4PBA
317 treatment also prevented loss of myogenic tone (Figure 5G and H) and significantly
318 diminished spontaneous ICH in 12 M-old *Col4a1*$^{+/G1344D}$ mice (Figure 5I and J). These
319 data suggest that 4PBA protects against age-dependent defects in myogenic tone and
320 ICH in *Col4a1*$^{+/G1344D}$ mice.

321 **Discussion**

322 Despite the enormous impact of the disease, the molecular pathogenesis of
323 cSVD is essentially unknown. Here we utilized the *Col4a1*$^{+/G1344D}$ mouse model of Gould
324 syndrome to investigate how this monogenic form of cSVD damages small arteries in
325 the brain during aging. Our findings show that these mice exhibit pathological changes
326 with age, including the loss of myogenic tone, high levels of spontaneous ICH, and brain
327 lesions. Electrophysiology experiments revealed that the loss of myogenic tone is

328 associated with diminished pressure-induced SMC depolarization and decreased
329 activities of BK and TRPM4 channels. In addition, we found that fundamental RyR- and
330 IP_3R-dependent Ca^{2+} signaling pathways are disrupted in SMCs from 12 M-old
331 *Col4a1*$^{+/G1344D}$ mice, likely due to a reduction in SR Ca^{2+} levels. Treating *Col4a1*$^{+/G1344D}$
332 mice with the chemical chaperone, 4PBA negated Ca^{2+} signaling disruptions, increased
333 BK and TRPM4 channel activity, prevented loss of myogenic tone, and reduced
334 spontaneous ICH. We conclude that the age-dependent cSVD pathogenesis of
335 *Col4a1*$^{+/G1344D}$ mice results from defects in SMC SR function that lead to reduced Ca^{2+}
336 store load and disrupted intracellular Ca^{2+} signaling. Defects in subcellular Ca^{2+} signals
337 diminish BK and TRPM4 channel activity, disrupting membrane potential regulation and
338 impeding pressure-induced constriction of cerebral arteries. These findings reveal a
339 novel mechanism that contributes to age-dependent cSVD.

340 Myogenic constriction protects delicate capillaries in the brain from pressure
341 overload during increases in cardiac output and perfusion associated with exercise,
342 stress, and other stimuli [14]. This vital response is deficient in several monogenetic forms
343 of cSVD [22,30,48]. However, the defects responsible for the loss of myogenic tone differ
344 between disease models. For example, Dabertrand *et al*. linked the loss of myogenic
345 tone in the CADASIL model with blunted pressure-induced SMC membrane potential
346 depolarization and connected the defect in membrane potential regulation with
347 increased surface expression of K_V channels and elevated hyperpolarizing K^+ current
348 density [22]. Notably, depletion of the minor membrane phospholipid PIP_2, leading to the
349 loss of TRPM4 channel activity, is the fundamental defect responsible for the loss of
350 myogenic constriction in a distinct mouse model of Gould syndrome caused by a

351 *Col4a1*^{G394V} mutation [30]. The current study uncovered a distinctive flaw in the SMCs of
352 *Col4a1*$^{+/G1344D}$ cSVD mice – impaired Ca^{2+} signaling. Our data show that the release of
353 Ca^{2+} from the SR through RyRs and IP_3Rs became faulty in *Col4a1*$^{+/G1344D}$ mice by 12
354 M of age. Impaired SR Ca^{2+} release disrupted the activity of BK and TRPM4 channels.
355 BK and TRPM4 channels play opposing roles in regulating SMC membrane potential
356 and contractility. TRPM4 channels depolarize the membrane and promote contractility,
357 whereas BK channels provide negative feedback to limit the magnitude of this response
358 [49]. When pressure-induced membrane depolarization is impaired, the BK pathway is
359 disengaged and has minimal influence on membrane potential [50].

360 Diminished levels of Ca^{2+} in the SR likely cause Ca^{2+} signaling and ion channel
361 defects in SMCs from 12 M-old *Col4a1*$^{+/G1344D}$. This concept is supported by prior
362 studies showing that a ~16% decrease in SR [Ca^{2+}] diminished STOC frequency by
363 70% and that a >20% decrease in SR [Ca^{2+}] completely abolished IP_3R-mediated Ca^{2+}
364 release in native SMCs [51,52]. In many types of cells, store-operated Ca^{2+} entry (SOCE)
365 is protective against decreases in ER/SR [Ca^{2+}] [53]. However, SOCE is virtually
366 undetectable in native, contractile vascular SMCs, promoting their susceptibility to
367 pathogenic SR Ca^{2+} depletion [50,54,55]. We conclude that SR Ca^{2+} store depletion and the
368 resultant dysregulation of BK, TRPM4, and SMC membrane potential is responsible for
369 the age-related loss of myogenic tone in *Col4a1*$^{+/G1344D}$ cSVD mice.

370 Steady-state free Ca^{2+} levels in the ER/SR are maintained by the release of Ca^{2+}
371 into the cytosol through RyRs and IP_3Rs, mobile and stationary Ca^{2+}-binding proteins in
372 the SR lumen, and transport of Ca^{2+} from the cytosol into the SR by sarco/endoplasmic
373 reticulum ATPase (SERCA) enzymes [46]. Disruption of one or more of these elements

374 could lead to SR Ca^{2+} defects in *Col4a1*$^{+/G1344D}$ mice. Interestingly, *Col4a1*$^{+/G1344D}$ mice
375 display impaired secretion and increased intracellular accumulation of collagen
376 α1α1α2(IV), presumably due to difficulties associated with the trafficking of misfolding of
377 mutant proteins out of the ER/SR [13]. The retention of misfolded proteins causes a
378 pathological condition known as ER/SR stress [56] that is associated with the depletion of
379 Ca^{2+} stores [57]. For example, Yamato *et al.* [58] demonstrated that tunicamycin-induced
380 ER stress promotes RyR-mediated Ca^{2+} leak, potentially due to increased reactive
381 oxygen species (ROS) production. Our data showed that treatment with a molecular
382 chaperone prevented SR Ca^{2+} handling defects and loss of myogenic tone and
383 significantly attenuated spontaneous ICH. These data provide evidence that ER/SR
384 stress contributes to SMC Ca^{2+} signaling defects and cSVD pathology of *Col4a1*$^{+/G1344D}$
385 mice. The age dependency of the disease process may reflect the normal functional
386 decline in SR protein homeostasis that is exacerbated by mutant collagen in the SR.

387 We conclude that age-dependent disruption of Ca^{2+} signaling in SMCs due to SR
388 stress and diminished SR Ca^{2+} store load contributes to cSVD pathology in
389 *Col4a1*$^{+/G1344D}$ mice. Future investigations into links between SMC SR stress and Ca^{2+}
390 handling defects in other genetic and sporadic forms of cSVD may provide insight into
391 novel pathogenic mechanisms.

392

393

394

395 **Materials and Methods**

396 **Chemical and reagents:** All chemicals and other reagents were obtained from Sigma-
397 Aldrich, Inc. (St. Louis, MO, USA) unless otherwise specified.

398 **Animals:** Young adult (~3M) and middle-aged (~12M) male and female littermate
399 *Col4a1*$^{+/+}$ and *Col4a1*$^{+/G1344D}$ mice were used in this study. The *Col4a1*^{G1344D} mutation
400 was backcrossed to C57BL/6J mice for over 20 generations [59]. Animals were
401 maintained in individually ventilated cages (≤5 mice/cage) with *ad libitum* access to food
402 and water in a room with controlled 12-hour light and dark cycles. All animal care
403 procedures and experimental protocols involving animals complied with the National
404 Institutes of Health (NIH) *Guide for the Care and Use of Laboratory Animals* and were
405 approved by the Institutional Animal Care and Use Committees at the University of
406 Nevada, Reno, and University of California, San Francisco.

407 **4PBA treatment:** Mice were provided with 4-phenylbutyrate (4PBA; 50 mM;
408 Scandinavian Formulas Inc., Sellersville, PA, USA) from birth in drinking water that was
409 refreshed weekly as described previously [26].

410 **Histological analysis:** Isoflurane anesthetized mice were transcardially perfused with
411 ice-cold phosphate-buffered saline (PBS) followed by ice-cold 4% paraformaldehyde
412 (Fisher, Waltham, MA, USA) in PBS. Brains were postfixed with 4% paraformaldehyde
413 for 24 hours at 4°C, cryoprotected in 30% sucrose in PBS, and embedded in optimal
414 cutting temperature compound (Fisher). Coronal cryosections (35 μm) regularly spaced
415 (500 μm) along the rostrocaudal axis were stained with a Prussian blue and nuclear fast
416 red stain kit (Abcam, Cambridge, UK) following the manufacturer's protocol. Images

417 were acquired with a BZ-X700 microscope using BZ-X Viewer 1.3.0.5 software and
418 stitched with BZ-X Analyzer 1.3.0.3 software (Keyence, Osaka, Japan). The percentage
419 of brain area with Prussian blue staining for each section was calculated with ImageJ
420 software (v2.3.0/1.53f; NIH, Bethesda, MD, USA). Hemorrhage severity was expressed
421 as the average percentage of hemosiderin surface area on ~21 sections for each brain.

422 ***In vivo* magnetic resonance imaging:** All *in vivo* magnetic resonance (MR)
423 experiments were conducted on a 14.1 Tesla vertical MR system (Agilent Technologies,
424 Palo-Alto, CA) equipped with 100 G/cm gradients and a single tuned millipede ^{1}H proton
425 coil ($Ø_I$ = 40 mm). For each imaging session, mice were anesthetized using isoflurane
426 (1-1.5% in O_2), positioned in a dedicated cradle maintaining constant anesthesia, and
427 placed in the MR bore; respiration and temperature were continuously monitored during
428 all acquisitions to ensure animal well-being and data reproducibility. Susceptibility
429 weighted imaging (SWI) was performed to acquire high-resolution images of the mouse
430 brain using the following parameters: gradient-echo scheme, field of view (FOV) = 20x
431 20 mm^2, matrix = 256 x 256, 16 slices, 0.4 mm slice thickness, 0.1 mm interslice gap,
432 number of averages = 16, echo time (TE)/repetition time (TR) = 4.60/140ms, flip angle =
433 10 degrees. T2-weighted (T2W) images were also acquired in a fast-spin-echo scheme
434 to evaluate anatomical brain structures, using the same FOV geometry as SWI and the
435 following parameters: number of averages = 8, TE/TR = 21.38/2500ms, flip angle = 90
436 degrees. The fast-spin-echo based T2W imaging is less sensitive to distortion artifacts
437 caused by B_0 inhomogeneity than SWI and is thus used for the atlas-based brain
438 structure registration as described below.

439 Using in-house software, hypointense lesions corresponding to ICH were
440 quantified based on manual segmentation of the SWI images. To investigate the
441 number and distribution of hypointense SWI lesions across the brain, an open-sourced
442 atlas-based imaging data analysis pipeline (AIDAmri) [60] was customized to register T2W
443 brain images to the Allen Brain Reference Atlas [61]. Based on the registration result, the
444 normalized lesion volumes for each brain region were summed up across all animals,
445 and an intra-group region-wise volumetric analysis was performed.

446 **Isolation of cerebral arteries and SMCs:** Mice were euthanized by decapitation under
447 isoflurane anesthesia. Cerebral arteries were carefully isolated from the brain in Ca^{2+}-
448 free Mg^{2+} physiological saline solution (Mg^{2+}-PSS) consisting of 140 mM NaCl, 5 mM
449 KCl, 2 mM $MgCl_2$, 10 mM HEPES, and 10 mM glucose (pH 7.4, adjusted with NaOH),
450 with 0.5% bovine serum albumin (BSA). Native SMCs for patch-clamp experiments
451 were obtained by initially digesting isolated arteries in 1 mg/mL papain (Worthington
452 Biochemical Corporation, Lakewood, NJ, USA), 1 mg/mL dithiothreitol (DTT), and 10
453 mg/mL BSA in Ca^{2+}-free PSS at 37°C for 12 minutes, followed by a 14-minute
454 incubation with 1 mg/mL type II collagenase (Worthington Biochemical Corporation). A
455 single-cell suspension was prepared by washing digested arteries three times with
456 Mg^{2+}-PSS and triturating with a fire-polished glass pipette. All cells used for this study
457 were freshly dissociated on the day of experimentation.

458 **Pressure myography:** The current best practice guidelines for pressure myography
459 experiments were followed [32]. Arteries were mounted between two glass cannulas
460 (outer diameter, 40–50 μm) in a pressure myograph chamber (Living Systems
461 Instrumentation, St Albans City, VT, USA) and secured by a nylon thread. Intraluminal

462 pressure was controlled using a servo-controlled peristaltic pump (Living Systems
463 Instrumentation), and preparations were visualized with an inverted microscope (Accu-
464 Scope Inc., Commack, NY, USA) coupled to a USB camera (The Imaging Source LLC,
465 Charlotte, NC, USA). Changes in luminal diameter were assessed using IonWizard
466 software (version 7.2.7.138; IonOptix LLC, Westwood, MA, USA). Arteries were bathed
467 in warmed (37°C), oxygenated (21% O_2, 6% CO_2, 73% N_2) PSS (119 mM NaCl, 4.7 mM
468 KCl, 21 mM $NaHCO_3$, 1.17 mM $MgSO_4$, 1.8 mM $CaCl_2$, 1.18 mM KH_2PO_4, 5 mM
469 glucose, 0.03 mM EDTA) at an intraluminal pressure of 5 mmHg. Following equilibration
470 for 15 min, intraluminal pressure was increased to 110 mmHg, and vessels were
471 stretched to their approximate *in vivo* length, after which pressure was reduced back to
472 5 mmHg for an additional 15 min. Vessel viability was assessed for each preparation by
473 evaluating vasoconstriction response to high extracellular [K^+] PSS, made isotonic by
474 adjusting the [NaCl] (60 mM KCl, 63.7 mM NaCl). Arteries that showed less than 10%
475 constriction in response to elevated [K^+] were excluded from further investigation.

476 Myogenic tone was assessed by raising the intraluminal pressure stepwise from
477 5 mmHg to 120 mmHg in 20 mmHg increments (5 to 20 mmHg for the first step). The
478 active diameter was obtained by allowing vessels to equilibrate for at least 5 minutes at
479 each pressure or until a steady-state diameter was reached. Following completion of the
480 pressure-response study, intraluminal pressure was lowered to 5 mmHg, and arteries
481 were superfused with Ca^{2+}-free PSS supplemented with EGTA (2 mM) and the voltage-
482 dependent Ca^{2+} channel blocker diltiazem (10 μM) to inhibit SMC contraction, after
483 which passive diameter was obtained by repeating the stepwise increase in intraluminal

484 pressure. Myogenic tone at each pressure step was calculated as myogenic tone (%) =
485 [1 – (active lumen diameter/passive lumen diameter)] × 100.

486 **Membrane potential:** For measurements of SMC membrane potential, cerebral arteries
487 were isolated, cannulated, and viability confirmed as described above. SMC membrane
488 potential was recorded from intact pressurized arteries at intraluminal pressures of 20
489 mmHg and 80 mmHg. SMCs were impaled through the adventitia with glass intracellular
490 microelectrodes (100-200 MΩ) backfilled with 3M KCl. Membrane potential was
491 recorded using an Electro 705 amplifier (World Precision Instruments, Sarasota, FL,
492 USA). Analog output from the amplifier was recorded using Ionwizard software (version
493 7.5.1.162; IonOptix). Criteria for acceptance of membrane potential recordings were 1)
494 an abrupt negative deflection of potential as the microelectrode was advanced into a
495 cell, 2) stable membrane potential for at least 30 seconds, and 3) an abrupt change in
496 the potential to ~0 mV after the electrode was retracted from the cell.

497 **Electrophysiological recordings:** Enzymatically isolated native SMCs were
498 transferred to a recording chamber (Warner Instruments, Holliston, MA, USA) and
499 allowed to adhere to glass coverslips for 20 minutes at room temperature. Recording
500 electrodes (3–5 MΩ) were pulled on a model P-87 micropipette puller (Sutter
501 Instruments, Novato, CA, USA) and polished using a MF-830 MicroForge (Narishige
502 Scientific Instruments Laboratories, Long Island, NY, USA). Currents were recorded at
503 room temperature using an Axopatch 200B amplifier (Molecular Devices, Sunnyvale,
504 CA, USA) equipped with an Axon CV 203BU headstage and Digidata 1440A digitizer
505 (Molecular Devices) for all patch-clamp electrophysiology experiments. Clampex and
506 Clampfit (version 10.2; Molecular Devices) were used for data acquisition and analysis.

507 The bathing solution composition for perforated-patch recordings of Kv currents,
508 STOCs, and TICCs was 134 mM NaCl, 6 mM KCl, 1 mM $MgCl_2$, 2 mM $CaCl_2$, 10 mM
509 HEPES, and 10 mM glucose (pH 7.4, adjusted with NaOH). The patch pipette solution
510 contained 110 mM K-aspartate, 1 mM $MgCl_2$, 30 mM KCl, 10 mM NaCl, 10 mM HEPES,
511 and 5 μM EGTA (pH 7.2, adjusted with KOH). Amphotericin B (200 μM) was included in
512 the pipette solution to gain electrical access. Whole-cell K^+ currents were recorded
513 using a step protocol (-60 to +60 mV in 10 mV, 250 ms steps) from a holding potential of
514 -80 mV. The BK channel blocker paxilline (1 μM) was included in the bath solution when
515 Kv currents were recorded. Whole-cell K^+ currents were recorded in the absence and
516 presence of K_V channel blocker 4-aminopyridine (5 mM), and the Kv component was
517 determined by subtraction. Summary current-voltage (I-V) plots were generated using
518 values obtained from the last 50 ms of each step. STOCs were recorded from SMCs
519 voltage-clamped over a range of membrane potentials (-60 to 0 mV; 10 mV steps).
520 TICCs were recorded from SMCs voltage-clamped at -70 mV; membrane stretch was
521 delivered by applying negative pressure through the recording electrode using a
522 pressure clamp system (HSPC-1; ALA Scientific Instruments Inc., Farmingdale, NY,
523 USA). TICC activity was calculated as the sum of the open channel probability (NP_o) of
524 multiple open states of 1.75 pA [62].

525 Whole-cell TRPM4 currents were recorded in a bath solution consisting of 156
526 mM NaCl, 1.5 mM $CaCl_2$, 10 mM glucose, 10 mM HEPES, and 10 mM TEACl (pH 7.4,
527 adjusted with NaOH). The patch pipette solution contained 156 mM CsCl, 8 mM NaCl,
528 1 mM $MgCl_2$, 10 mM HEPES (pH 7.4, adjusted with NaOH), and a free Ca^{2+}
529 concentration of 200 μM, adjusted using the appropriate amount of $CaCl_2$ and EGTA, as

530 determined with Max-Chelator software (WEBMAXC standard, available at
531 https://somapp.ucdmc.ucdavis.edu/pharmacology/bers/maxchelator/webmaxc/webmaxc
532 S.htm. Whole-cell cation currents were evoked by applying 400 ms voltage ramps from -
533 100 to +100 mV from a holding potential of -60 mV. Voltage ramps were repeated every
534 2 s for 300 s. The selective TRPM4 inhibitor 9-phenanthrol (30 μM) was applied after
535 peak TRPM4 current was recorded (~100 s). Whole-cell TRPM4 current amplitude was
536 expressed as the 9-phenanthrol-sensitive current at +100 mV.

537 **Quantitative droplet digital PCR:** Total RNA was extracted from isolated cerebral
538 arteries by homogenization in TRIzol reagent (Invitrogen, Waltham, MA, USA), followed
539 by purification using a Direct-zol RNA microprep kit (Zymo Research, Irvine, CA, USA)
540 with on-column DNAse treatment. RNA concentration was determined using an RNA
541 6000 Pico Kit run on a Bioanalyzer 2100 running Agilent 2100 Expert Software
542 (B.02.11; Agilent Technologies, Santa Clara, CA, USA). RNA was converted to cDNA
543 using iScript cDNA Supermix (Bio-Rad, Hercules, CA, USA). Quantitative droplet digital
544 PCR (ddPCR) was performed using QX200 ddPCR EvaGreen Supermix (Bio-Rad),
545 custom-designed primers (Supplementary Table 1), and cDNA templates. Generated
546 droplet emulsions were amplified using a C100 Touch Thermal Cycler (Bio-Rad), and
547 the fluorescence intensities of individual droplets were measured using a QX200
548 Droplet Reader (Bio-Rad) running QuantaSoft (version 1.7.4; Bio-Rad). Analysis was
549 performed using QuantaSoft Analysis Pro (version 1.0596; Bio-Rad).

550 **Ca^{2+} imaging:** Images were acquired using an iXon 897 EMCCD camera (Andor; 16 ×
551 16 μm pixel size) coupled to a spinning-disk confocal head (CSU-X1; Yokogawa) with a
552 100× oil-immersion objective (Olympus; NA 1.45) at an acquisition rate of 33 frames per

553 second (fps). Custom software (SparkAn; https://github.com/vesselman/SparkAn)
554 provided by Dr. Adrian D. Bonev (University of Vermont) was used to analyze the
555 properties of Ca^{2+} sparks and whole-cell RyR and IP_3R Ca^{2+} signals.

556 To image Ca^{2+} sparks, a suspension of freshly isolated SMCs was placed in a glass-
557 bottom 35 mm dish, and cells were allowed to adhere to the glass coverslip for 20 min
558 at room temperature. SMCs were then loaded with the Ca^{2+}-sensitive fluorophore, Fluo-
559 4-AM (1 μM; Invitrogen), in the dark for 20 minutes at room temperature in Mg^{2+}-PSS.
560 Cells were subsequently washed three times with Ca^{2+}-containing PSS and incubated
561 at room temperature for 20 min in the dark to allow sufficient time for Fluo-4 de-
562 esterification. The threshold for Ca^{2+} spark detection was defined as local increases in
563 fluorescence $\geq 0.2\ \Delta F/F_0$.

564 To image RyR and IP_3R Ca^{2+} signals, SMCs were plated and loaded with Fluo-4-AM as
565 stated above, but immediately before imaging, cells were washed three times and
566 imaged in Mg^{2+}-PSS to eliminate signals resulting from the influx of Ca^{2+}. Caffeine (10
567 mM) or U46619 (100 nM; Enzo Biochem, Farmingdale, NY) were applied to the bath.

568 **Statistical analysis:** All summary data are presented as means ± SEM. Statistical
569 analyses were performed, and graphs were constructed using Prism version 9.3.1
570 (GraphPad Software, San Diego, CA, USA). The value of n refers to the number of cells
571 for patch-clamp electrophysiology and Ca^{2+} imaging experiments, the number of
572 arteries for pressure myography and membrane potential experiments, and the number
573 of animals for histological analyses, magnetic resonance imaging, and ddPCR
574 experiments. Statistical analyses were performed using unpaired Student's t-tests and

575 one-way and two-way analysis of variance (ANOVA). A P value < 0.05 was considered
576 statistically significant for all analyses.

577 **Grant support:** This study was supported by grants from the National Institutes of
578 Health (NHLBI R35HL155008, R01HL091905, R01HL137852, R01HL139585,
579 R01146054, and R01HL122770, NIGMS P20GM130459 to S.E., and NINDS
580 RF1NS110044 and R33NS115132 to M.M.C, D.B.G, and S.E.; The Transgenic
581 Genotyping and Phenotyping Core at the COBRE Center for Molecular and Cellular
582 Signaling in the Cardiovascular System, University of Nevada, Reno, is maintained by a
583 grant from NIH/NIGMS (P20GM130459 Sub#5451), as is the High Spatial and
584 Temporal Resolution Imaging Core at the COBRE Center for Molecular and Cellular
585 Signaling in the Cardiovascular System, University of Nevada, Reno (P20GM130459
586 Sub#5452). The UCSF Department of Ophthalmology is supported by P30EY002162
587 and an unrestricted grant from Research to Prevent Blindness. This study was also
588 supported by a grant from the American Heart Association (23CDA1054627 to P.T.).

589 **Author contributions:** S.E. and D.B.G. initiated and supervised the project. S.E.
590 designed the experiments. E.Y. performed brain histology, pressure myography, sharp
591 electrode and patch-clamp electrophysiology, Ca^{2+} imaging, and ddPCR experiments.
592 X.W. and X.G. performed magnetic resonance imaging experiments. S.A. and A.S.S.
593 performed patch-clamp electrophysiology experiments. P.T. performed pressure
594 myography experiments. C.L.D. performed animal colony management. E.Y., S.A.,
595 A.S.S., P.T., X.G., and S.E. analyzed the data. E.Y. and S.E. drafted the manuscript
596 and prepared the figures. E.Y., C.L.D, M.M.C., D.B.G., and S.E. revised the manuscript.

597 **Competing interests**: The authors declare that they have no competing interests.

Data and materials availability: All data needed to evaluate the conclusions in the paper are present in the paper or the Supplementary Materials

Figures

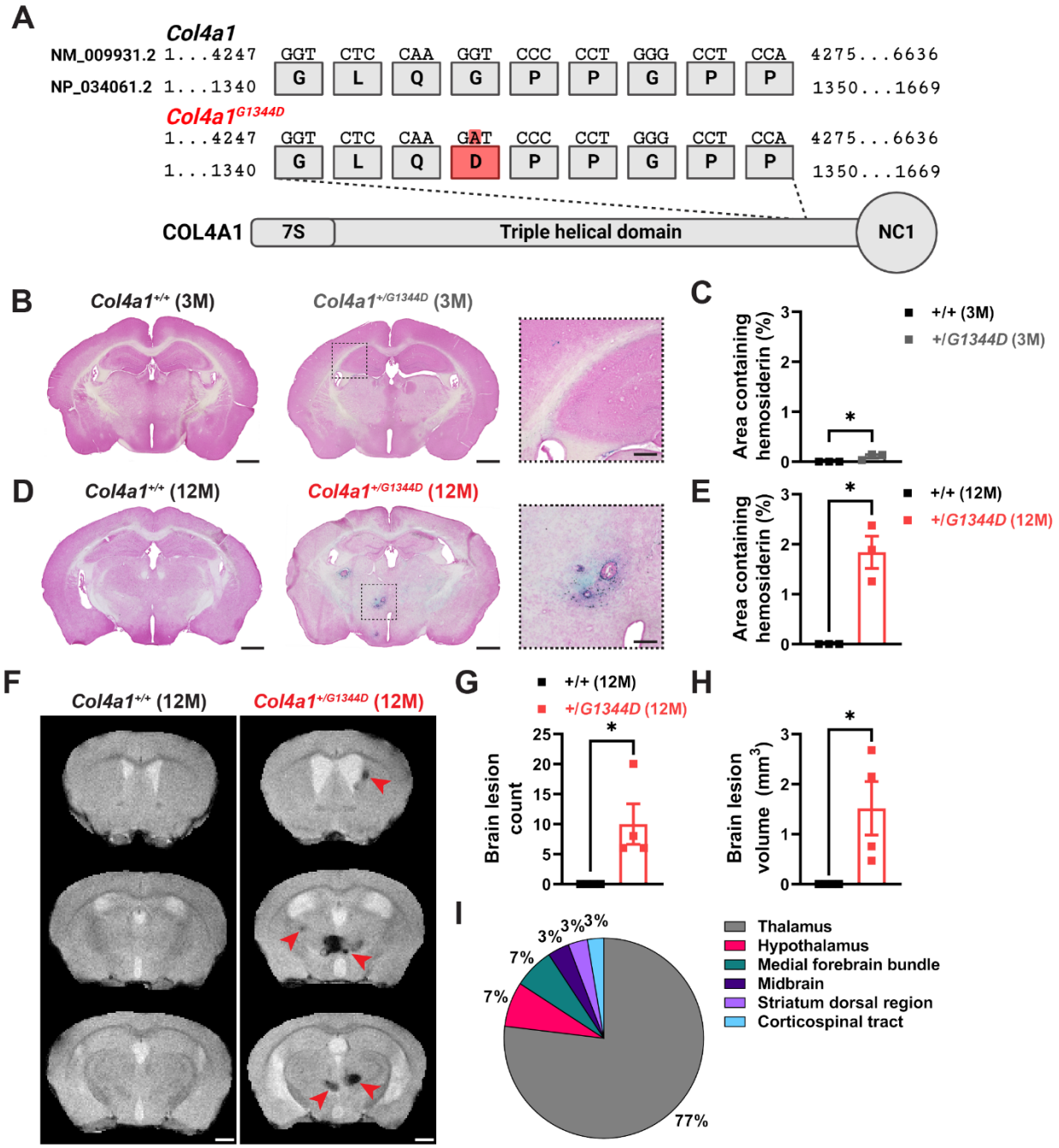

Figure 1. *Col4a1*$^{+/G1344D}$ mice exhibit age-dependent pathologies. (A) Schematic representation of the *Col4a1* point mutation that leads to *Col4a1*^{G1344D}. **(B)** Intracerebral hemorrhage (ICH) was assessed using Prussian blue staining. Representative images

605 of brain sections from 3 M-old *Col4a1*$^{+/+}$ and *Col4a1*$^{+/G1344D}$ mice stained with Prussian
606 blue. **(C)** Summary data presented as percentage of brain area with Prussian blue
607 staining in brain sections (500 μm intervals). N = 3 animals per group. *P ≤ 0.05,
608 unpaired t-test. **(D)** Representative images of brain sections from 12 M-old *Col4a1*$^{+/+}$
609 and *Col4a1*$^{+/G1344D}$ mice stained with Prussian blue. **(E)** Summary data presented as
610 percentage of brain area with Prussian blue staining in brain sections (500 μm
611 intervals). N = 3 animals per group. *P ≤ 0.05, unpaired t-test. **(F)** Brain lesions were
612 evaluated *in vivo* using high-field susceptibility-weighted magnetic resonance imaging
613 (SWI). Representative SWI images from 12 M-old *Col4a1*$^{+/+}$ and *Col4a1*$^{+/G1344D}$ mice.
614 Red arrowheads highlight hypointense pixels that indicate hemorrhagic lesions.
615 Quantification of **(G)** the number of lesions and **(H)** the total volume of lesions detected
616 by SWI. N = 4 animals per group. *P ≤ 0.05, unpaired t-test. **(I)** Region-wise volumetric
617 distribution of lesions detected by SWI from 12 M-old *Col4a1*$^{+/G1344D}$ mice. Scale bars =
618 1 mm. Inset scale bars = 250 μm.

619

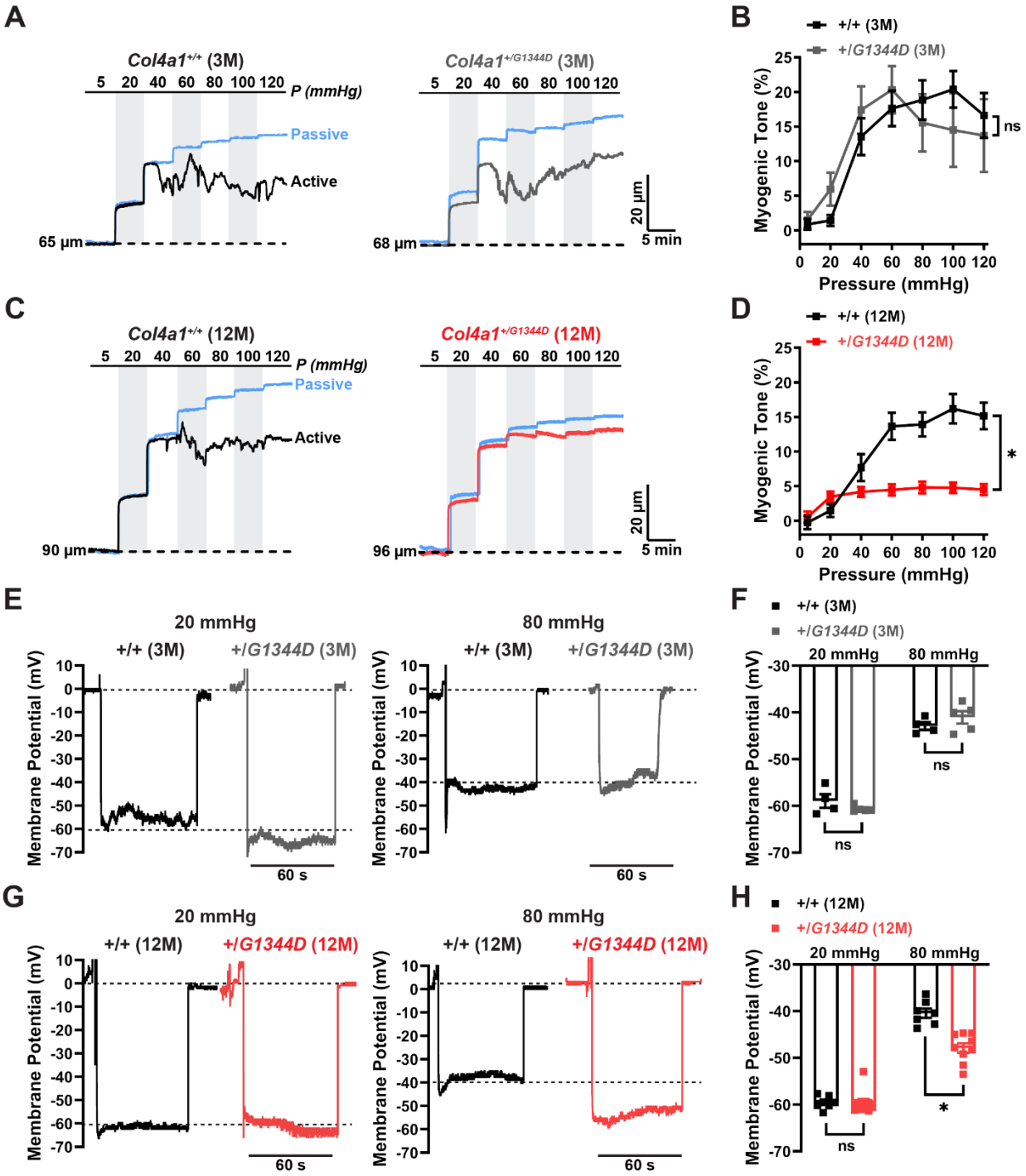

Figure 2. Diminished pressure-induced constriction of cerebral arteries from 12 M-old *Col4a1*$^{+/G1344D}$ mice is due to impaired SMC membrane depolarization. (A) Representative recordings of the inner diameter of isolated cerebral arteries from 3 M-

624 old *Col4a1*$^{+/+}$ and *Col4a1*$^{+/G1344D}$ mice show the myogenic response to increased
625 pressure (active) and the dilation of the same arteries when extracellular Ca^{2+} has been
626 removed (passive). **(B)** Summary data of myogenic tone as a function of intraluminal
627 pressure. n = 5-10 vessels from 5 or 6 animals per group. ns = not significant, two-way
628 ANOVA. **(C)** Representative recordings of the inner diameter of isolated cerebral
629 arteries from 12 M-old *Col4a1*$^{+/+}$ and *Col4a1*$^{+/G1344D}$ mice. **(D)** Summary data of
630 myogenic tone as a function of intraluminal pressure. n = 13 vessels from 6 or 9 animals
631 per group. *P ≤ 0.05, two-way ANOVA. **(E)** Representative membrane potential (mV)
632 recordings of smooth muscle cells (SMCs) in pressurized cerebral arteries isolated from
633 3 M-old *Col4a1*$^{+/+}$ and *Col4a1*$^{+/G1344D}$ mice at 20 mmHg and 80 mmHg intraluminal
634 pressure. **(F)** Summary data showing membrane potential of SMCs in pressurized
635 cerebral arteries at 20 mmHg and 80 mmHg intraluminal pressure. n = 4-5 vessels from
636 3 or 4 animals per group. ns = not significant, unpaired t-test. **(G)** Representative
637 membrane potential recordings of SMCs in pressurized cerebral arteries isolated from
638 12 M-old *Col4a1*$^{+/+}$ and *Col4a1*$^{+/G1344D}$ mice at 20 mmHg and 80 mmHg intraluminal
639 pressure. **(H)** Summary data showing membrane potential of SMCs in pressurized
640 cerebral arteries at 20 mmHg and 80 mmHg intraluminal pressure. n = 7-9 vessels from
641 5 or 6 mice per group. *P ≤ 0.05, unpaired t-test.

642

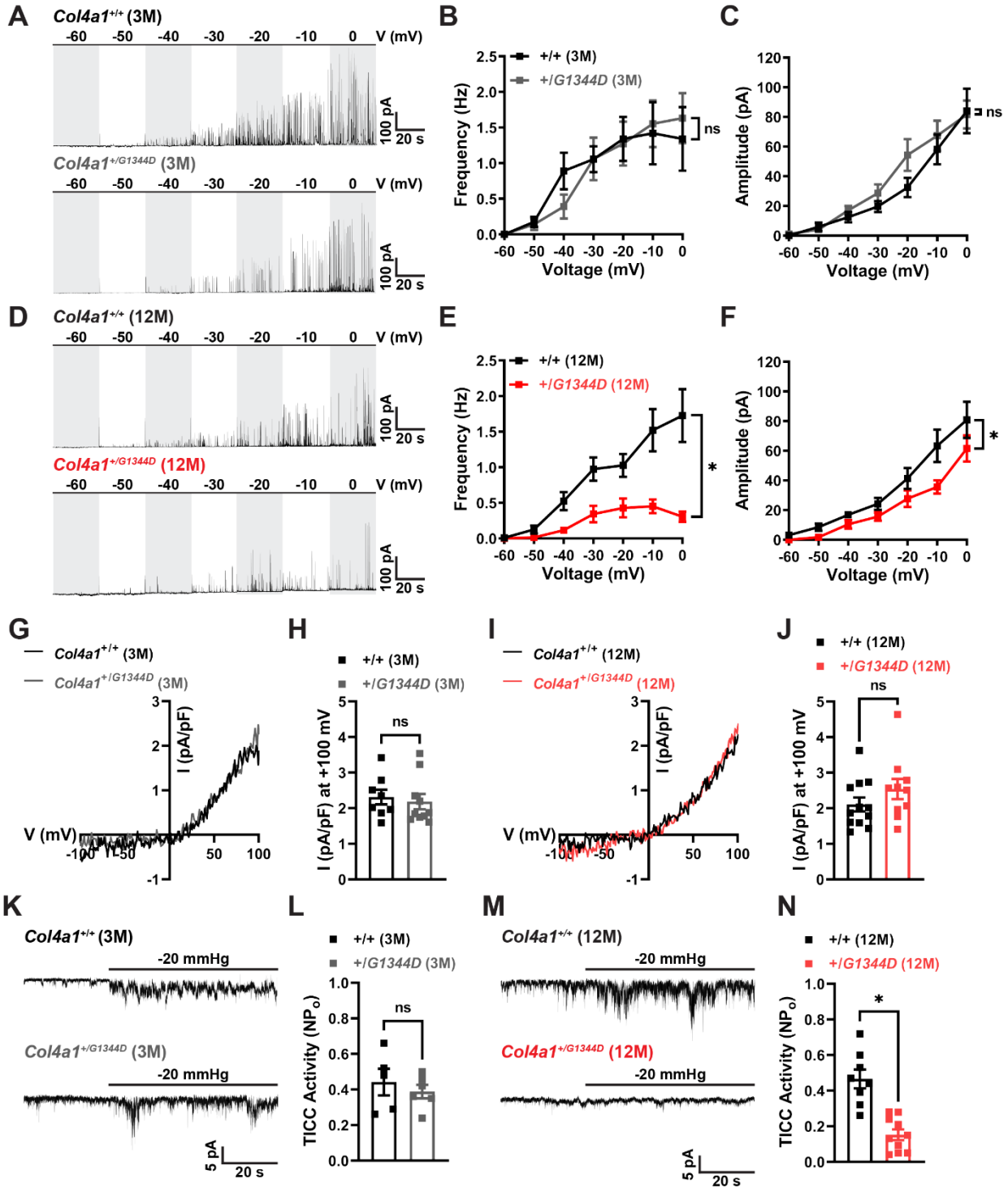

643

644 **Figure 3. Age-dependent declines in BK and TRPM4 channel activity in SMCs**

645 **from *Col4a1*$^{+/G1344D}$ mice. (A)** Representative traces of spontaneous transient outward

646 currents (STOCs) in freshly isolated cerebral artery smooth muscle cells (SMCs) from 3

647 M-old *Col4a1*$^{+/+}$ and *Col4a1*$^{+/G1344D}$ mice over a range of membrane potentials (-60 to 0
648 mV). Summary data showing STOC frequency **(B)** and amplitude **(C)** at each command
649 potential. n = 8-12 cells from 5 animals per group. ns = not significant, two-way ANOVA.
650 **(D)** Representative traces of STOCs in cerebral artery SMCs from 12 M-old *Col4a1*$^{+/+}$
651 and *Col4a1*$^{+/G1344D}$ mice. Summary data showing STOC frequency **(E)** and amplitude
652 **(F)** at each command potential. n = 12 cells from 5 animals per group. *P ≤ 0.05, two-
653 way ANOVA. **(G)** Representative I-V plots of whole-cell patch-clamp TRPM4 current
654 recordings during voltage ramps (-100 to 100 mV) in cerebral artery SMCs from 3 M-old
655 *Col4a1*$^{+/+}$ and *Col4a1*$^{+/G1344D}$ mice. Currents were evoked by including 200 μM free Ca^{2+}
656 in the intracellular solution, and the TRPM4 portion of the current was determined by
657 adding TRPM4 blocker 9-phenanthrol (30 μM). **(H)** Summary of whole-cell TRPM4
658 current density at +100 mV. n = 8-10 cells from 3 or 4 animals per group. ns = not
659 significant, unpaired t-test. **(I)** Representative I-V plots of whole-cell patch-clamp
660 TRPM4 current recordings in cerebral artery SMCs from 12 M-old *Col4a1*$^{+/+}$ and
661 *Col4a1*$^{+/G1344D}$ mice. **(J)** Summary of whole-cell TRPM4 current density at +100 mV. n =
662 10-12 cells from 4 animals per group. ns = not significant, unpaired t-test. **(K)**
663 Representative traces of transient inward cation currents (TICCs) evoked by applying
664 negative pressure (-20 mmHg) to stretch the plasma membrane of voltage-clamped (-70
665 mV) cerebral artery SMCs isolated from 3 M-old *Col4a1*$^{+/+}$ and *Col4a1*$^{+/G1344D}$ mice. **(L)**
666 Summary data of TICC activity. n = 5-6 cells from 3 animals per group. ns = not
667 significant, unpaired t-test. **(M)** Representative traces of TICCs in cerebral artery SMCs
668 isolated from 12 M-old *Col4a1*$^{+/+}$ and *Col4a1*$^{+/G1344D}$ mice. **(N)** Summary data of TICC
669 activity. n = 8-10 cells from 4 or 5 animals per group. *P ≤ 0.05, unpaired t-test.

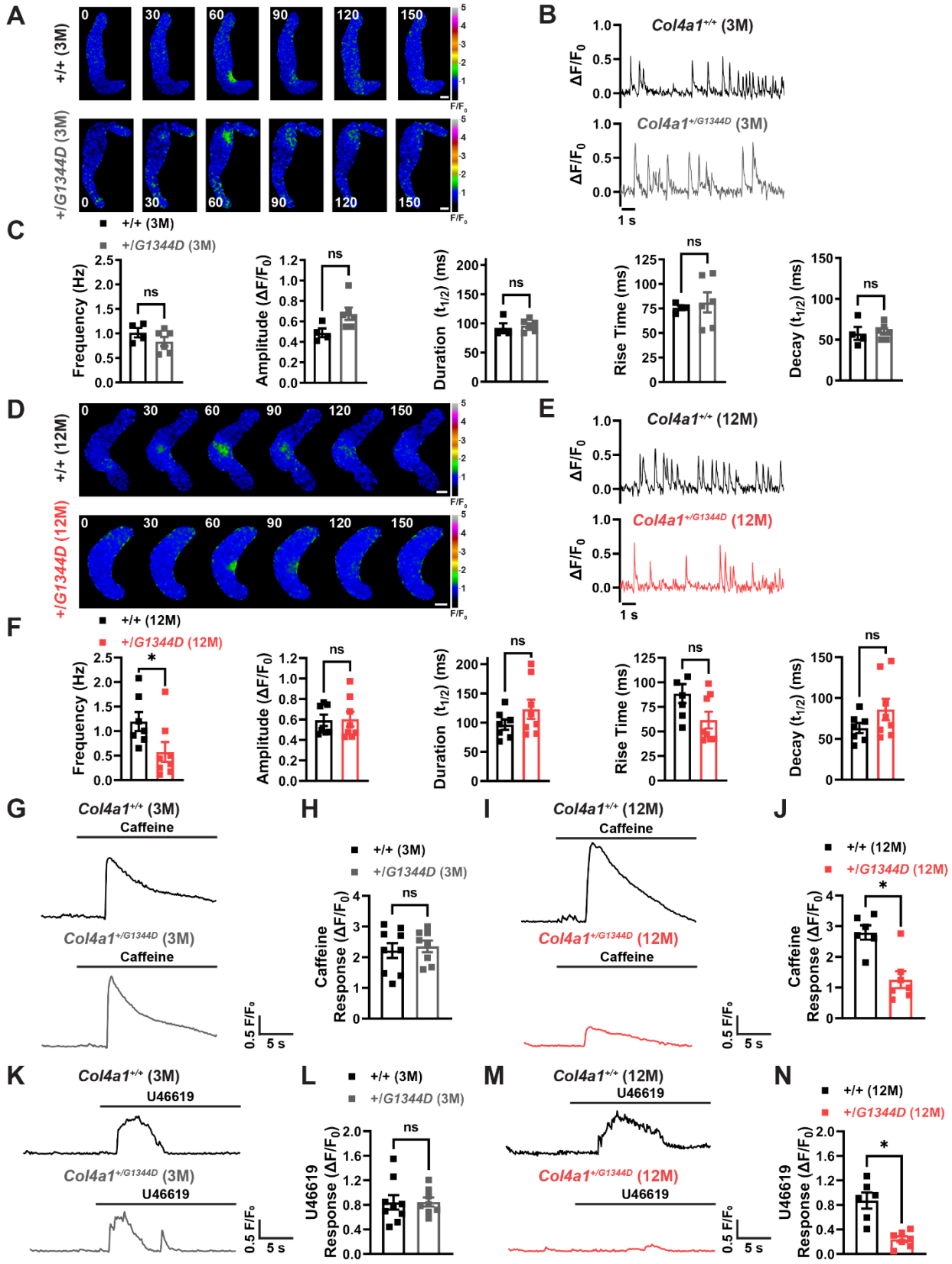
A
+/+ (3M)
+/G1344D (3M)
0
30
60
90
120
150
F/F0
B
Col4a1+/+ (3M)
Col4a1+/G1344D (3M)
ΔF/F0
1 s
C
+/+ (3M)
+/G1344D (3M)
Frequency (Hz)
Amplitude (ΔF/F0)
Duration (t1/2) (ms)
Rise Time (ms)
Decay (t1/2) (ms)
ns
D
+/+ (12M)
+/G1344D (12M)
E
Col4a1+/+ (12M)
Col4a1+/G1344D (12M)
F
+/+ (12M)
+/G1344D (12M)
*
G
Col4a1+/+ (3M)
Caffeine
Col4a1+/G1344D (3M)
0.5 F/F0
5 s
H
Caffeine Response (ΔF/F0)
I
Col4a1+/+ (12M)
Col4a1+/G1344D (12M)
J
K
U46619
L
U46619 Response (ΔF/F0)
M
N

670

671 **Figure 4. Defective intracellular Ca^{2+} signaling in cerebral artery SMCs from 12 M-**
672 **old *Col4a1*$^{+/G1344D}$ mice. (A)** Representative time-course spinning disk confocal images
673 exhibiting Ca^{2+} spark events in Fluo-4-AM loaded cerebral artery smooth muscle cells
674 (SMCs) from 3 M-old *Col4a1*$^{+/+}$ and *Col4a1*$^{+/G1344D}$ mice. Time = milliseconds, scale bar
675 = 5 µm. **(B)** Representative traces of Ca^{2+} spark events in cerebral artery SMCs isolated
676 from 3 M-old *Col4a1*$^{+/+}$ and *Col4a1*$^{+/G1344D}$ mice presented as changes in fractional
677 fluorescence ($\Delta F/F_0$) vs. time. **(C)** Summary data showing Ca^{2+} spark frequency,
678 amplitude, duration, rise time, and decay. n = 4-6 cells from 3 animals per group. ns =
679 not significant, unpaired t-test. **(D)** Representative time-course images exhibiting Ca^{2+}
680 spark events in cerebral artery SMCs from 12 M-old *Col4a1*$^{+/+}$ and *Col4a1*$^{+/G1344D}$. Time
681 = milliseconds, scale bar = 5 µm. **(E)** Representative traces of Ca^{2+} spark events in
682 cerebral artery SMCs isolated from 12 M-old *Col4a1*$^{+/+}$ and *Col4a1*$^{+/G1344D}$ mice
683 presented as $\Delta F/F_0$ vs. time. **(F)** Summary data showing Ca^{2+} spark frequency,
684 amplitude, duration, rise time, and decay. n = 7-8 cells from 3 or 4 animals per group. *P
685 ≤ 0.05, ns = not significant, unpaired t-test. **(G)** Representative traces showing whole-
686 cell F/F_0 changes in response to caffeine (10 mM) in Fluo-4-AM loaded cerebral artery
687 SMCs from 3 M-old *Col4a1*$^{+/+}$ and *Col4a1*$^{+/G1344D}$ mice. **(H)** Summary data of the $\Delta F/F_0$
688 in response to caffeine. n = 8-9 cells from 3 animals per group. ns = not significant,
689 unpaired t-test. **(I)** Representative traces showing whole-cell F/F_0 changes in response
690 to caffeine in SMCs from 12 M-old *Col4a1*$^{+/+}$ and *Col4a1*$^{+/G1344D}$ mice. **(J)** Summary data
691 of the $\Delta F/F_0$ in response to caffeine. n = 6-7 cells from 3 animals per group. *P ≤ 0.05,
692 unpaired t-test. **(K)** Representative traces showing whole-cell F/F_0 changes in response
693 to U46619 (100 nM) in Fluo-4-AM loaded cerebral artery SMCs from 3 M-old *Col4a1*$^{+/+}$

694 and *Col4a1*$^{+/G1344D}$ mice. **(L)** Summary data of the $\Delta F/F_0$ in response to U46619. n = 8-9

695 cells from 3 animals per group. ns = not significant, unpaired t-test. **(M)** Representative

696 traces showing whole-cell F/F_0 changes in response to U46619 in SMCs from 12 M-old

697 *Col4a1*$^{+/+}$ and *Col4a1*$^{+/G1344D}$ mice. **(N)** Summary data of the $\Delta F/F_0$ in response to

698 U46619. n = 6-7 cells from 3 animals per group. *$P \leq 0.05$, unpaired t-test.

699

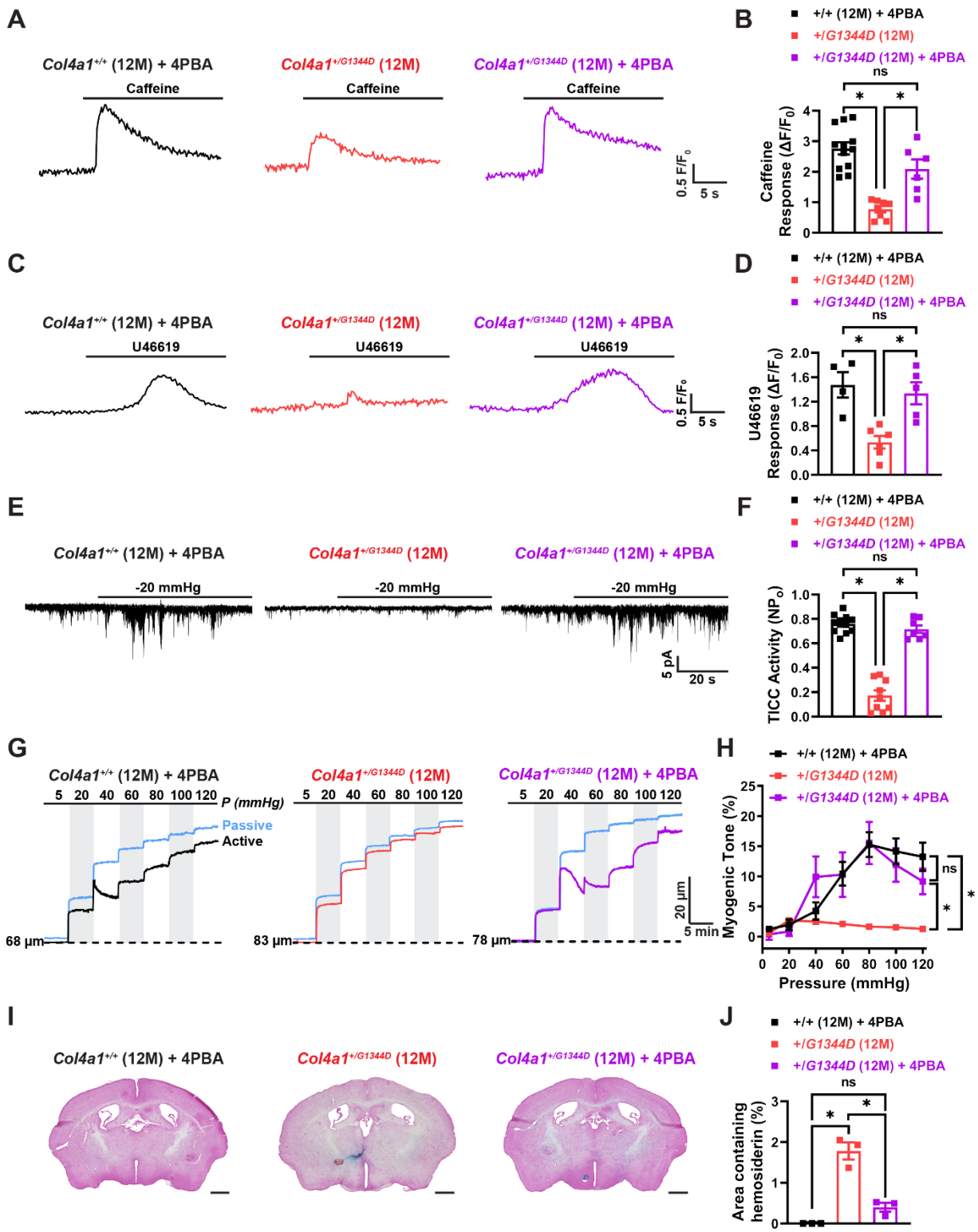

700

701 **Figure 5. 4PBA prevents age-related cerebral artery defects in *Col4a1*$^{+/G1344D}$ mice.**

702 **(A)** Representative traces showing whole-cell F/F$_0$ changes in response to caffeine (10

703 mM) in Fluo-4-AM loaded cerebral artery SMCs from 4PBA treated 12 M-old *Col4a1*$^{+/+}$
704 and *Col4a1*$^{+/G1344D}$ and untreated *Col4a1*$^{+/G1344D}$ mice. **(B)** Summary data of the $\Delta F/F_0$ in
705 response to caffeine. n = 6-12 cells from 3-4 animals per group. *P ≤ 0.05, ns = not
706 significant, one-way ANOVA. **(C)** Representative traces showing whole-cell F/F_0
707 changes in response to U46619 (100 nM) in Fluo-4-AM loaded cerebral artery SMCs
708 from 4PBA treated 12 M-old *Col4a1*$^{+/+}$ and *Col4a1*$^{+/G1344D}$ and untreated *Col4a1*$^{+/G1344D}$
709 mice. **(D)** Summary data of the $\Delta F/F_0$ in response to U46619. n = 4-6 cells from 3-4
710 animals per group. *P ≤ 0.05, ns = not significant, one-way ANOVA. **(E)** Representative
711 traces of transient inward cation currents (TICCs) evoked by applying negative pressure
712 (-20 mmHg) to stretch the plasma membrane of voltage-clamped (-70 mV) cerebral
713 artery SMCs isolated from 4PBA treated 12 M-old *Col4a1*$^{+/+}$ and *Col4a1*$^{+/G1344D}$ and
714 untreated *Col4a1*$^{+/G1344D}$ mice. **(F)** Summary data of TICC activity. n = 7-11 cells from 3-
715 4 animals per group. *P ≤ 0.05, ns = not significant, one-way ANOVA. **(G)**
716 Representative recordings of the inner diameter of isolated cerebral arteries from 4PBA-
717 treated 12 M-old *Col4a1*$^{+/+}$ and *Col4a1*$^{+/G1344D}$ and untreated *Col4a1*$^{+/G1344D}$ mice
718 showing the myogenic response to increases in pressure (active) and the dilation of the
719 same arteries when extracellular Ca^{2+} has been removed (passive). **(H)** Summary data
720 of myogenic tone as a function of intraluminal pressure. n = 6 or 9 vessels from 3 or 5
721 mice. *P ≤ 0.05, ns = not significant, two-way ANOVA. **(I)** Representative images of
722 Prussian blue stained brain sections from 4PBA treated 12 M-old *Col4a1*$^{+/+}$ and
723 *Col4a1*$^{+/G1344D}$ and untreated *Col4a1*$^{+/G1344D}$ mice. Scale bar = 1 mm. **(J)** Summary data
724 presented as percentage of brain area with Prussian blue staining in brain sections (500
725 μm intervals). N = 3 animals per group. *P ≤ 0.05, ns = not significant, one-way ANOVA.

726 **References Cited**

727 1. Markus HS. Genes, endothelial function and cerebral small vessel disease in
728 man. *Exp Physiol*. 2008;93:121-127. doi: 10.1113/expphysiol.2007.038752
729 2. Pantoni L. Cerebral small vessel disease: from pathogenesis and clinical
730 characteristics to therapeutic challenges. *Lancet Neurol*. 2010;9:689-701. doi:
731 10.1016/S1474-4422(10)70104-6
732 3. Choi JC. Genetics of cerebral small vessel disease. *J Stroke*. 2015;17:7-16. doi:
733 10.5853/jos.2015.17.1.7
734 4. Joutel A, Faraci FM. Cerebral small vessel disease: insights and opportunities
735 from mouse models of collagen IV-related small vessel disease and cerebral
736 autosomal dominant arteriopathy with subcortical infarcts and
737 leukoencephalopathy. *Stroke*. 2014;45:1215-1221. doi:
738 10.1161/STROKEAHA.113.002878
739 5. Joutel A, Haddad I, Ratelade J, Nelson MT. Perturbations of the cerebrovascular
740 matrisome: A convergent mechanism in small vessel disease of the brain? *J*
741 *Cereb Blood Flow Metab*. 2016;36:143-157. doi: 10.1038/jcbfm.2015.62
742 6. Rutten-Jacobs LC, Traylor M, Adib-Samii P, Thijs V, Sudlow C, Rothwell PM,
743 Boncoraglio G, Dichgans M, Bevan S, Meschia J, et al. Common NOTCH3
744 Variants and Cerebral Small-Vessel Disease. *Stroke*. 2015;46:1482-1487. doi:
745 10.1161/STROKEAHA.114.008540
746 7. Gould DB, Phalan FC, Breedveld GJ, van Mil SE, Smith RS, Schimenti JC,
747 Aguglia U, van der Knaap MS, Heutink P, John SW. Mutations in Col4a1 cause
748 perinatal cerebral hemorrhage and porencephaly. *Science*. 2005;308:1167-1171.
749 doi: 10.1126/science.1109418
750 8. Gould DB, Phalan FC, van Mil SE, Sundberg JP, Vahedi K, Massin P, Bousser
751 MG, Heutink P, Miner JH, Tournier-Lasserve E, et al. Role of COL4A1 in small-
752 vessel disease and hemorrhagic stroke. *N Engl J Med*. 2006;354:1489-1496. doi:
753 10.1056/NEJMoa053727
754 9. Lanfranconi S, Markus HS. COL4A1 mutations as a monogenic cause of cerebral
755 small vessel disease: a systematic review. *Stroke*. 2010;41:e513-518. doi:
756 10.1161/STROKEAHA.110.581918
757 10. Jeanne M, Jorgensen J, Gould DB. Molecular and Genetic Analyses of Collagen
758 Type IV Mutant Mouse Models of Spontaneous Intracerebral Hemorrhage
759 Identify Mechanisms for Stroke Prevention. *Circulation*. 2015;131:1555-1565.
760 doi: 10.1161/CIRCULATIONAHA.114.013395
761 11. Jeanne M, Labelle-Dumais C, Jorgensen J, Kauffman WB, Mancini GM, Favor J,
762 Valant V, Greenberg SM, Rosand J, Gould DB. COL4A2 mutations impair
763 COL4A1 and COL4A2 secretion and cause hemorrhagic stroke. *Am J Hum*
764 *Genet*. 2012;90:91-101. doi: 10.1016/j.ajhg.2011.11.022
765 12. Gould DB, Marchant JK, Savinova OV, Smith RS, John SW. Col4a1 mutation
766 causes endoplasmic reticulum stress and genetically modifiable ocular
767 dysgenesis. *Hum Mol Genet*. 2007;16:798-807. doi: 10.1093/hmg/ddm024
768 13. Kuo DS, Labelle-Dumais C, Mao M, Jeanne M, Kauffman WB, Allen J, Favor J,
769 Gould DB. Allelic heterogeneity contributes to variability in ocular dysgenesis,

770 myopathy and brain malformations caused by Col4a1 and Col4a2 mutations.
771 *Hum Mol Genet*. 2014;23:1709-1722. doi: 10.1093/hmg/ddt560
772 14. Davis MJ, Hill MA. Signaling mechanisms underlying the vascular myogenic
773 response. *Physiol Rev*. 1999;79:387-423. doi: 10.1152/physrev.1999.79.2.387
774 15. Gonzales AL, Garcia ZI, Amberg GC, Earley S. Pharmacological inhibition of
775 TRPM4 hyperpolarizes vascular smooth muscle. *Am J Physiol Cell Physiol*.
776 2010;299:C1195-1202. doi: 10.1152/ajpcell.00269.2010
777 16. Earley S, Waldron BJ, Brayden JE. Critical role for transient receptor potential
778 channel TRPM4 in myogenic constriction of cerebral arteries. *Circ Res*.
779 2004;95:922-929. doi: 10.1161/01.RES.0000147311.54833.03
780 17. Reading SA, Brayden JE. Central role of TRPM4 channels in cerebral blood flow
781 regulation. *Stroke*. 2007;38:2322-2328. doi: 10.1161/STROKEAHA.107.483404
782 18. Nelson MT, Cheng H, Rubart M, Santana LF, Bonev AD, Knot HJ, Lederer WJ.
783 Relaxation of arterial smooth muscle by calcium sparks. *Science*. 1995;270:633-
784 637. doi: 10.1126/science.270.5236.633
785 19. Knot HJ, Standen NB, Nelson MT. Ryanodine receptors regulate arterial
786 diameter and wall [Ca2+] in cerebral arteries of rat via Ca2+-dependent K+
787 channels. *J Physiol*. 1998;508 (Pt 1):211-221. doi: 10.1111/j.1469-
788 7793.1998.211br.x
789 20. Jackson WF. Potassium Channels in Regulation of Vascular Smooth Muscle
790 Contraction and Growth. *Adv Pharmacol*. 2017;78:89-144. doi:
791 10.1016/bs.apha.2016.07.001
792 21. Gonzales AL, Amberg GC, Earley S. Ca2+ release from the sarcoplasmic
793 reticulum is required for sustained TRPM4 activity in cerebral artery smooth
794 muscle cells. *Am J Physiol Cell Physiol*. 2010;299:C279-288. doi:
795 10.1152/ajpcell.00550.2009
796 22. Dabertrand F, Kroigaard C, Bonev AD, Cognat E, Dalsgaard T, Domenga-Denier
797 V, Hill-Eubanks DC, Brayden JE, Joutel A, Nelson MT. Potassium
798 channelopathy-like defect underlies early-stage cerebrovascular dysfunction in a
799 genetic model of small vessel disease. *Proc Natl Acad Sci U S A*.
800 2015;112:E796-805. doi: 10.1073/pnas.1420765112
801 23. Murray LS, Lu Y, Taggart A, Van Regemorter N, Vilain C, Abramowicz M, Kadler
802 KE, Van Agtmael T. Chemical chaperone treatment reduces intracellular
803 accumulation of mutant collagen IV and ameliorates the cellular phenotype of a
804 COL4A2 mutation that causes haemorrhagic stroke. *Hum Mol Genet*.
805 2014;23:283-292. doi: 10.1093/hmg/ddt418
806 24. Malo A, Kruger B, Goke B, Kubisch CH. 4-Phenylbutyric acid reduces
807 endoplasmic reticulum stress, trypsin activation, and acinar cell apoptosis while
808 increasing secretion in rat pancreatic acini. *Pancreas*. 2013;42:92-101. doi:
809 10.1097/MPA.0b013e318259f6ca
810 25. Perlmutter DH. Chemical chaperones: a pharmacological strategy for disorders
811 of protein folding and trafficking. *Pediatr Res*. 2002;52:832-836. doi:
812 10.1203/00006450-200212000-00004
813 26. Hayashi G, Labelle-Dumais C, Gould DB. Use of sodium 4-phenylbutyrate to
814 define therapeutic parameters for reducing intracerebral hemorrhage and

815 myopathy in Col4a1 mutant mice. *Dis Model Mech*. 2018;11. doi:
816 10.1242/dmm.034157
817 27. Cannistraro RJ, Badi M, Eidelman BH, Dickson DW, Middlebrooks EH, Meschia
818 JF. CNS small vessel disease: A clinical review. *Neurology*. 2019;92:1146-1156.
819 doi: 10.1212/WNL.0000000000007654
820 28. Hilal S, Mok V, Youn YC, Wong A, Ikram MK, Chen CL. Prevalence, risk factors
821 and consequences of cerebral small vessel diseases: data from three Asian
822 countries. *J Neurol Neurosurg Psychiatry*. 2017;88:669-674. doi: 10.1136/jnnp-
823 2016-315324
824 29. Meuwissen ME, Halley DJ, Smit LS, Lequin MH, Cobben JM, de Coo R, van
825 Harssel J, Sallevelt S, Woldringh G, van der Knaap MS, et al. The expanding
826 phenotype of COL4A1 and COL4A2 mutations: clinical data on 13 newly
827 identified families and a review of the literature. *Genet Med*. 2015;17:843-853.
828 doi: 10.1038/gim.2014.210
829 30. Yamasaki E, Ali S, Sanchez Solano A, Thakore P, Smith M, Wang X, Labelle-
830 Dumais C, Gould DB, Earley S. Faulty TRPM4 channels underlie age-dependent
831 cerebral vascular dysfunction in Gould syndrome. *Proc Natl Acad Sci U S A*.
832 2023;120:e2217327120. doi: 10.1073/pnas.2217327120
833 31. Shi Y, Wardlaw JM. Update on cerebral small vessel disease: a dynamic whole-
834 brain disease. *Stroke Vasc Neurol*. 2016;1:83-92. doi: 10.1136/svn-2016-000035
835 32. Wenceslau CF, McCarthy CG, Earley S, England SK, Filosa JA, Goulopoulou S,
836 Gutterman DD, Isakson BE, Kanagy NL, Martinez-Lemus LA, et al. Guidelines for
837 the measurement of vascular function and structure in isolated arteries and
838 veins. *Am J Physiol Heart Circ Physiol*. 2021;321:H77-H111. doi:
839 10.1152/ajpheart.01021.2020
840 33. Harder DR. Pressure-dependent membrane depolarization in cat middle cerebral
841 artery. *Circ Res*. 1984;55:197-202. doi: 10.1161/01.res.55.2.197
842 34. Knot HJ, Nelson MT. Regulation of arterial diameter and wall [Ca2+] in cerebral
843 arteries of rat by membrane potential and intravascular pressure. *J Physiol*.
844 1998;508 (Pt 1):199-209. doi: 10.1111/j.1469-7793.1998.199br.x
845 35. Pritchard HAT, Gonzales AL, Pires PW, Drumm BT, Ko EA, Sanders KM, Hennig
846 GW, Earley S. Microtubule structures underlying the sarcoplasmic reticulum
847 support peripheral coupling sites to regulate smooth muscle contractility. *Sci*
848 *Signal*. 2017;10. doi: 10.1126/scisignal.aan2694
849 36. Brayden JE, Nelson MT. Regulation of arterial tone by activation of calcium-
850 dependent potassium channels. *Science*. 1992;256:532-535. doi:
851 10.1126/science.1373909
852 37. Launay P, Fleig A, Perraud AL, Scharenberg AM, Penner R, Kinet JP. TRPM4 is
853 a Ca2+-activated nonselective cation channel mediating cell membrane
854 depolarization. *Cell*. 2002;109:397-407. doi: 10.1016/s0092-8674(02)00719-5
855 38. Gonzales AL, Yang Y, Sullivan MN, Sanders L, Dabertrand F, Hill-Eubanks DC,
856 Nelson MT, Earley S. A PLCgamma1-dependent, force-sensitive signaling
857 network in the myogenic constriction of cerebral arteries. *Sci Signal*. 2014;7:ra49.
858 doi: 10.1126/scisignal.2004732

859 39. Earley S, Straub SV, Brayden JE. Protein kinase C regulates vascular myogenic
860 tone through activation of TRPM4. *Am J Physiol Heart Circ Physiol*.
861 2007;292:H2613-2622. doi: 10.1152/ajpheart.01286.2006
862 40. Nilius B, Prenen J, Droogmans G, Voets T, Vennekens R, Freichel M,
863 Wissenbach U, Flockerzi V. Voltage dependence of the Ca2+-activated cation
864 channel TRPM4. *J Biol Chem*. 2003;278:30813-30820. doi:
865 10.1074/jbc.M305127200
866 41. Pires PW, Ko EA, Pritchard HAT, Rudokas M, Yamasaki E, Earley S. The
867 angiotensin II receptor type 1b is the primary sensor of intraluminal pressure in
868 cerebral artery smooth muscle cells. *J Physiol*. 2017;595:4735-4753. doi:
869 10.1113/JP274310
870 42. Yamasaki E, Thakore P, Krishnan V, Earley S. Differential expression of
871 angiotensin II type 1 receptor subtypes within the cerebral microvasculature. *Am*
872 *J Physiol Heart Circ Physiol*. 2020;318:H461-H469. doi:
873 10.1152/ajpheart.00582.2019
874 43. Schleifenbaum J, Kassmann M, Szijarto IA, Hercule HC, Tano JY, Weinert S,
875 Heidenreich M, Pathan AR, Anistan YM, Alenina N, et al. Stretch-activation of
876 angiotensin II type 1a receptors contributes to the myogenic response of mouse
877 mesenteric and renal arteries. *Circ Res*. 2014;115:263-272. doi:
878 10.1161/CIRCRESAHA.115.302882
879 44. Yasuda N, Miura S, Akazawa H, Tanaka T, Qin Y, Kiya Y, Imaizumi S, Fujino M,
880 Ito K, Zou Y, et al. Conformational switch of angiotensin II type 1 receptor
881 underlying mechanical stress-induced activation. *EMBO Rep*. 2008;9:179-186.
882 doi: 10.1038/sj.embor.7401157
883 45. McPherson PS, Kim YK, Valdivia H, Knudson CM, Takekura H, Franzini-
884 Armstrong C, Coronado R, Campbell KP. The brain ryanodine receptor: a
885 caffeine-sensitive calcium release channel. *Neuron*. 1991;7:17-25. doi:
886 10.1016/0896-6273(91)90070-g
887 46. Wray S, Burdyga T. Sarcoplasmic reticulum function in smooth muscle. *Physiol*
888 *Rev*. 2010;90:113-178. doi: 10.1152/physrev.00018.2008
889 47. Iannitti T, Palmieri B. Clinical and experimental applications of sodium
890 phenylbutyrate. *Drugs R D*. 2011;11:227-249. doi: 10.2165/11591280-
891 000000000-00000
892 48. Joutel A, Monet-Lepretre M, Gosele C, Baron-Menguy C, Hammes A, Schmidt S,
893 Lemaire-Carrette B, Domenga V, Schedl A, Lacombe P, et al. Cerebrovascular
894 dysfunction and microcirculation rarefaction precede white matter lesions in a
895 mouse genetic model of cerebral ischemic small vessel disease. *J Clin Invest*.
896 2010;120:433-445. doi: 10.1172/JCI39733
897 49. Nelson MT, Quayle JM. Physiological roles and properties of potassium channels
898 in arterial smooth muscle. *Am J Physiol*. 1995;268:C799-822. doi:
899 10.1152/ajpcell.1995.268.4.C799
900 50. Krishnan V, Ali S, Gonzales AL, Thakore P, Griffin CS, Yamasaki E, Alvarado
901 MG, Johnson MT, Trebak M, Earley S. STIM1-dependent peripheral coupling
902 governs the contractility of vascular smooth muscle cells. *Elife*. 2022;11. doi:
903 10.7554/eLife.70278

51. McCarron JG, Craig JW, Bradley KN, Muir TC. Agonist-induced phasic and tonic responses in smooth muscle are mediated by InsP(3). *J Cell Sci*. 2002;115:2207-2218. doi: 10.1242/jcs.115.10.2207
52. Shmygol A, Wray S. Modulation of agonist-induced Ca2+ release by SR Ca2+ load: direct SR and cytosolic Ca2+ measurements in rat uterine myocytes. *Cell Calcium*. 2005;37:215-223. doi: 10.1016/j.ceca.2004.10.002
53. Parekh AB, Putney JW, Jr. Store-operated calcium channels. *Physiol Rev*. 2005;85:757-810. doi: 10.1152/physrev.00057.2003
54. Fernandez RA, Wan J, Song S, Smith KA, Gu Y, Tauseef M, Tang H, Makino A, Mehta D, Yuan JX. Upregulated expression of STIM2, TRPC6, and Orai2 contributes to the transition of pulmonary arterial smooth muscle cells from a contractile to proliferative phenotype. *Am J Physiol Cell Physiol*. 2015;308:C581-593. doi: 10.1152/ajpcell.00202.2014
55. Potier M, Gonzalez JC, Motiani RK, Abdullaev IF, Bisaillon JM, Singer HA, Trebak M. Evidence for STIM1- and Orai1-dependent store-operated calcium influx through ICRAC in vascular smooth muscle cells: role in proliferation and migration. *FASEB J*. 2009;23:2425-2437. doi: 10.1096/fj.09-131128
56. Schroder M, Kaufman RJ. The mammalian unfolded protein response. *Annu Rev Biochem*. 2005;74:739-789. doi: 10.1146/annurev.biochem.73.011303.074134
57. Lebeau PF, Platko K, Byun JH, Austin RC. Calcium as a reliable marker for the quantitative assessment of endoplasmic reticulum stress in live cells. *J Biol Chem*. 2021;296:100779. doi: 10.1016/j.jbc.2021.100779
58. Yamamoto WR, Bone RN, Sohn P, Syed F, Reissaus CA, Mosley AL, Wijeratne AB, True JD, Tong X, Kono T, et al. Endoplasmic reticulum stress alters ryanodine receptor function in the murine pancreatic beta cell. *J Biol Chem*. 2019;294:168-181. doi: 10.1074/jbc.RA118.005683
59. Favor J, Gloeckner CJ, Janik D, Klempt M, Neuhauser-Klaus A, Pretsch W, Schmahl W, Quintanilla-Fend L. Type IV procollagen missense mutations associated with defects of the eye, vascular stability, the brain, kidney function and embryonic or postnatal viability in the mouse, Mus musculus: an extension of the Col4a1 allelic series and the identification of the first two Col4a2 mutant alleles. *Genetics*. 2007;175:725-736. doi: 10.1534/genetics.106.064733
60. Pallast N, Diedenhofen M, Blaschke S, Wieters F, Wiedermann D, Hoehn M, Fink GR, Aswendt M. Processing Pipeline for Atlas-Based Imaging Data Analysis of Structural and Functional Mouse Brain MRI (AIDAmri). *Front Neuroinform*. 2019;13:42. doi: 10.3389/fninf.2019.00042
61. Dong HW. *Allen reference atlas : a digital color brain atlas of the C57Black/6J male mouse*. Hoboken, N.J.: Wiley; 2008.
62. Gonzales AL, Amberg GC, Earley S. Ca2+ release from the sarcoplasmic reticulum is required for sustained TRPM4 activity in cerebral artery smooth muscle cells. *American journal of physiology Cell physiology*. 2010;299:C279-288.